Author Manuscript

Author Manuscript

Author Manuscript

Author Manuscript

HHS Public Access

Author manuscript

J Physiol. Author manuscript; available in PMC 2024 April 01.

Published in final edited form as:

J Physiol. 2023 April ; 601(7): 1183–1206. doi:10.1113/JP284171.

Intestinal distension orchestrates neuronal activity in the enteric nervous system of adult mice

Jean-Baptiste Cavin[1,2,3,4,*,†], **Preedajit Wongkrasant**[1,2,3,4,*], **Joel B. Glover**[1,5], **Onesmo B. Balemba**[6], **Wallace K. MacNaughton**[1,3,4], **Keith A. Sharkey**[1,2,4,‡]

[1]Snyder Institute for Chronic Diseases

[2]Hotchkiss Brain Institute

[3]Inflammation Research Network

[4]Department of Physiology & Pharmacology

[5]Live Cell Imaging Laboratory, Cumming School of Medicine, University of Calgary, Calgary, Alberta, Canada

[6]Department of Biological Sciences, University of Idaho, Moscow, ID, USA.

Abstract

The enteric nervous system (ENS) regulates the motor, secretory and defensive functions of the gastrointestinal tract. Enteric neurons integrate mechanical and chemical inputs from the gut lumen to generate complex motor outputs. How intact enteric neural circuits respond to changes in the gut lumen is not well understood. We recorded intracellular calcium in live-cell confocal recordings in neurons from intact segments of mouse intestine in order to investigate neuronal response to luminal mechanical and chemical stimuli. Wnt1-, ChAT- and Calb1-GCaMP6 mice were used to record neurons from the jejunum and colon. We measured neuronal calcium response to KCl (75 mM), veratridine (10 μM), DMPP (100 μM) or luminal nutrients (Ensure®), in the presence or absence of intraluminal distension. In the jejunum and colon, distension generated by the presence of luminal content (chyme or fecal pellets, respectively) renders the underlying enteric circuit unresponsive to depolarizing stimuli. In the distal colon, high levels of distension inhibit neuronal response to KCl, while intermediate levels of distension reorganize

‡Corresponding author: Dr. Keith Sharkey, Department of Physiology and Pharmacology, Cumming School of Medicine, University of Calgary, 3330 Hospital Drive NW, Calgary, Alberta, T2N 4N1, Canada, ksharkey@ucalgary.ca, Tel: 587-578-6097.

*Contributed equally to this work

†Author's current address: Department of Gastrointestinal Health, Nestlé Institute of Health Science, Lausanne, Switzerland

Author Contributions

J-BC, KAS and WKM designed the studies, J-BC and JG designed and built the chambers, J-BC and PW conducted the experiments and performed data analyses. OBB provided critical tools essential for the study. J-BC drafted the manuscript, all authors critically revised and approved the final manuscript for submission. All authors agree to be accountable for all aspects of the work in ensuring that questions related to the accuracy or integrity of any part of the work are appropriately investigated and resolved and all persons designated as authors qualify for authorship, and all those who qualify for authorship are listed.

Supporting Information

Supplementary Figure: Supporting information on chamber design. Supplementary material: Chamber STL file, Chamber mold STL file, Tissue stabilizer STL file, Retaining clip STL file and explanatory text file (Imaging Chamber 3DModels).

Additional information

Competing interests

All authors declare they have no conflicts of interest related to any aspect of this work.

Author Manuscript Author Manuscript Author Manuscript Author Manuscript

Ca^{2+} response in circumferentially propagating slow waves. Mechanosensitive channel inhibition suppresses distension-induced Ca^{2+} elevations and calcium-activated potassium channel inhibition restores neuronal response to KCl, but not DMPP in the distended colon. In the jejunum, distension prevents a previously unknown tetrodotoxin-resistant neuronal response to luminal nutrient stimulation. Our results demonstrate that intestinal distension regulates the excitability of ENS circuits via mechanosensitive channels. Physiological levels of distension locally silence or synchronize neurons, dynamically regulating the excitability of enteric neural circuits based on the content of the intestinal lumen.

Live, 3-dimensional calcium (Ca^{2+}) recordings were made in intact segments of the jejunum, proximal and distal colon in mice expressing a genetically encoded Ca^{2+} indicator (GCaMP6) in the enteric nervous system (ENS). In the undistended region of the colon (as well other segments), intracellular Ca^{2+} is low and neurons respond simultaneously to a depolarizing stimulus (KCl). When distension increases, intracellular Ca^{2+} increases and neurons respond in circumferential waves. In the fully distended colon, the neuronal response is lost. Distension is integrated by mechanosensitive ion channels, including the calcium-activated potassium channel $K_{Ca1.1}$ that regulates intracellular Ca^{2+} in the ENS. In presence of distension, responses to depolarizing stimuli (KCl and veratridine), the nicotinic receptor agonist (DMPP) or luminal nutrients (jejunum only) are lost.

Graphical Abstract

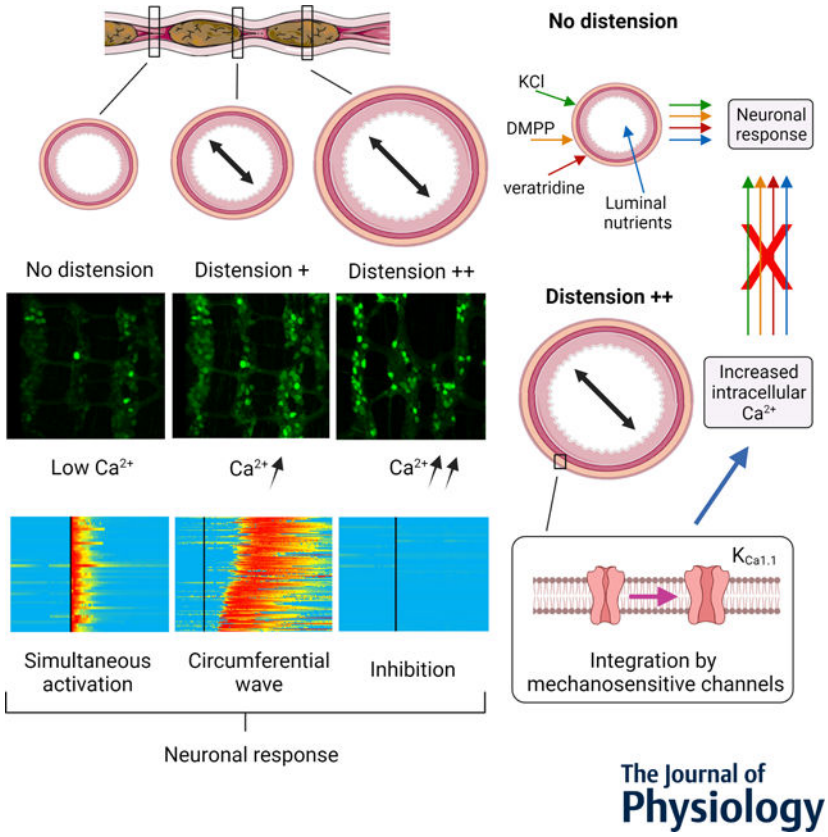

Author Manuscript Author Manuscript Author Manuscript Author Manuscript

Keywords

Enteric nervous system; calcium imaging; myenteric plexus; submucosal plexus; jejunum; colon; mechanosensitive channels

Introduction

The gastrointestinal tract has the complex task of moving food along its length and mixing the contents to facilitate digestion and the absorption of nutrients and water. In order to regulate these processes and to integrate them into the body's homeostatic control networks, the gastrointestinal tract is endowed with an extensive intrinsic innervation as well as an extrinsic autonomic and primary afferent innervation (Furness, 2012; Sharkey & Mawe, 2022). Extrinsic, vagal (Williams et al., 2016; Kaelberer et al., 2018; Pradhananga et al., 2020) and spinal afferent (Lai et al., 2020) pathways react to a variety of stimuli including stretch, nutrients and bacterial products to control both gut functions (Williams et al., 2016; Obata et al., 2020) and behaviour (Suarez et al., 2018; Han et al., 2018). The intrinsic innervation of the gut, the enteric nervous system (ENS), regulates motor and secretory activities by detecting and responding to changes in the luminal contents of the gastrointestinal tract (Furness, 2012; Spencer & Hu, 2020; Sharkey & Mawe, 2022). Using traditional dissected preparations, where neurons are exposed by removing either the inner mucosal or outer muscle layers, enteric neurons have been shown to respond to a variety of nutrient and microbial signals (Kunze et al., 1995, 2009; Bertrand et al., 1997; Bellono et al., 2017), as well as mechanical signals, including stretch, distension and compression (Mazzuoli & Schemann, 2012; Spencer et al., 2002). Dissected preparations have laid the groundwork for an understanding of the various components of the enteric circuitries; however, these preparations do not recapitulate the complexity of the combined mechanical and chemical stimulation received by the intact ENS during digestion. The recent development of imaging techniques and genetically encoded fluorescent reporters now facilitates the evaluation of neuronal activity in intact intestinal segments containing complete enteric circuits (Hennig et al., 2015; Boesmans et al., 2015). However, using these models in combination with chemical and mechanical stimulation is challenging. As a result, we have only a partial understanding of how the ENS integrates luminal signals. Innovative models are needed to evaluate the effect of the physiologically relevant mechanical and chemical stimulation on ENS function.

Here we designed an integrated imaging and analysis system allowing us to evaluate enteric neural network activity in intact intestinal segments from mice, while controlling the amount of distension and perfusing nutrients within the gut lumen. Using this tool, we discovered that intestinal distension plays a major role in regulating the activity and responsiveness of the ENS. Specifically, we showed that intestinal distension, generated artificially or by the presence of luminal content, inhibited the response to depolarizing stimuli in the ENS. This distension-induced quiescence was observed in the jejunum, proximal colon and distal colon. In the distal colon, we showed that the response to distension was mediated by mechanosensitive channels and more specifically calcium-activated potassium channels ($K_{Ca1.1}$ channels). The primarily affected neurons were

Author Manuscript Author Manuscript Author Manuscript Author Manuscript

shown to be choline acetyltransferase (ChAT) expressing neurons. We also showed that intermediate level distension, as observed at the outer limits of fecal pellets, led to a highly dynamic and reversible synchronization of signal propagation within the enteric nervous system. Finally, we uncovered a tetrodotoxin (TTX)-resistant response of enteric neurons to luminal nutrients in the jejunum. This response to nutrient was more specifically observed in calbindin 1 (Calb1)-expressing neurons and was totally inhibited in presence of luminal distension. Together our work unveils the critical regulatory role played by intestinal distension in signal integration by the ENS and highlights the crucial function of mechanosensitive channels in this regulation.

Materials and Methods

Ethical approval

This study was approved by the Health Sciences Animal Care Committee of the University of Calgary (Animal use protocol number: AC15–0129) and experimental protocols were carried out in accordance with the guidelines of the Canadian Council on Animal Care. The animal experiments conducted also comply with the policy and regulations of *The Journal of Physiology* (Grundy, 2015).

Animals and tissues

Breeders were purchased from the Jackson laboratory (Bar Harbor, ME, USA). B6;129S6-Gt(ROSA)$^{26Sortm96(CAG-GCaMP6s)Hze}$/J mice (Jackson 024106) were bred to homozygosity and then crossed with either 129S4.Cg-E2f1$^{Tg(Wnt1-cre)2Sor}$/J mice (Jackson 022137) or B6;129S-Calb1$^{tm2.1(cre)Hze}$/J mice (Jackson 028532) in order to generate Wnt1-GCaMP6 or Calb1-GCaMP6 mice, respectively at the University of Calgary. ChAT-GCaMP6 were bred at the University of Idaho by crossing female B6J.Cg-Gt(ROSA)26Sor$^{tm95.1(CAG-GCaMP6f)Hze}$/MwarJ (Jackson 028865), which express the Cre-dependent GCaMP6f protein with either male B6J.129S6-Chat$^{tm2(cre)Lowl/Mwar/J}$ (Jackson 028861). Animal procedures were approved by the University of Idaho Animal Care and Use Committee under animal protocol number IACUC-2021–14. Adult F1 mice were shipped to the University of Calgary following regulations of both institutions. Adult male and female mice (aged 2 to 8 months) were used. Mice were group housed (2–4 mice per cage) under a 12 h light–dark cycle (lights off at 19:00 h) in a temperature- and humidity-controlled room. Mice were allowed free access to a standard diet (LabDiet, St. Louis, MO, USA; 5061) and to tap water. All animals were euthanized by cervical dislocation under deep anesthesia (4% isoflurane, 96% O_2 in induction chamber). Intact 4–5 cm intestinal segments of jejunum (sampled 10 cm from the pylorus), proximal colon (sampled immediately after the caecum) and distal colon (sampled proximally from the rectum) were removed immediately after euthanasia. Intestinal segments were either cleaned of luminal content or mounted in the chambers with their luminal content (fecal pellet or chyme) left intact.

Imaging chambers

A custom-made perfusion chamber was designed to image the intestinal segments on an inverted confocal microscope (Fig. 1; Supporting information on chamber design). The

Author Manuscript Author Manuscript Author Manuscript Author Manuscript

chamber allows for independent control of the extraluminal and luminal media through separate inlet and outlet ports (Fig. 1A). It also features a tissue stabilizer and retaining clips to improve spatial stability, reduce vibration and minimize drift during image acquisition (Supporting information on chamber design). The chamber mold, tissue stabilizer and retaining clips were designed using Fusion 360 (2.0.8609, Autodesk, San Rafael, CA, USA) and fabricated using additive manufacturing and polymer casting. The main chamber bodies were made by pouring SYLGARD^{tm} 184 (Dow, Midland, MI, USA) into a mold and allowing it to cure at room temperature for 48 h before demolding (Supporting information on chamber design). STL files for the different components of the chambers (chamber, chamber mold, tissue stabilizer and retaining clips) are available in the Supplementary material). Molded chambers present the advantage of being easily replaceable to avoid cross-experiment contaminations with non-washable pharmacological agents. The mold was fabricated from thermoplastic polyurethane (NinjaFlex, Fenner Inc., Manheim, PA, USA) using a 3D printer (TAZ 4/5, LulzBot, Fargo, North Dakota, USA). In order to improve the stability of the preparation, we designed a tissue stabilizer preventing upward movement and protecting the intestinal segment from the bath flow (Supporting information on chamber design). The tissue stabilizer was manufactured using a 3D printer (Ultimaker 3, Ultimaker, Utrecht, Netherlands) with a polyamide copolymer material (Taulman3D Alloy 910, Filaments.ca, Mississauga, Ontario, Canada). Due to the elasticity of the chamber material, a retaining clip system was designed to couple the chamber assembly to the microscope stage (Supporting information on chamber design). This deflects potential vibrations from the perfused fluid through the clips and into the stage rather than into the chamber during imaging, thus reducing imaging artefacts and preventing spills. The retaining clips were manufactured using a 3D printer (Ultimaker 3) with a polylactic acid material (Ultimaker PLA). To assemble the system, vacuum grease was first applied to the chamber lip where the coverslip rests to form the imaging window. A 18×18–1 coverslip (Fisher Scientific Pittsburgh, PA, USA) was gently placed on the lip and light pressure was then applied to the coverslip to form a seal around the imaging window perimeter.

Calcium imaging

Intact intestinal segments were placed in the chamber as illustrated (Fig. 1A), cannulated at both ends and tied with surgical thread. The assembled chamber was then mounted on the microscope stage as illustrated and connected to the input/output flow circuits. The tissues were bathed at 35–37°C, in oxygenated (95 % O_2, 5 % CO_2) Krebs solution containing (in mmol.L^{-1}): 121 NaCl, 5.9 KCl, 2.5 $CaCl_2$, 1.2 $MgCl_2$, 1.2 NaH_2PO_4, 14.4 $NaHCO_3$, 11 glucose (Sigma) with 3 μmol.L^{-1} nicardipine and 1 μmol.L^{-1} scopolamine (Sigma-Aldrich, St Louis, USA) to inhibit smooth muscle contractions, as previously described(Gulbransen et al., 2012). Constant flow and temperature in the bath were maintained using a Minipuls 3 peristaltic pump (Gilson, Middleton, WI, USA) and a TC-344B heater controller (Harvard Apparatus, Holliston, MA, USA). Tissues were allowed to equilibrate for 10 to 15 minutes before the beginning of the experiments. For luminal perfusion experiments, the intestinal segments were perfused with non-oxygenated Krebs solution (to keep the lumen anoxic) at 10 mL.h^{-1} during the equilibration period and the intraluminal flow rate was maintained constant for the duration of the experiment. Intraluminal flow and temperature were maintained constant using PHD 2000 syringe pumps (Harvard Apparatus) combined with

Author Manuscript Author Manuscript Author Manuscript Author Manuscript

1LG Syringe heaters (New Era Pump Systems Inc, Farmingdale, NY, USA) to infuse and withdraw solutions from the oral and anal end of the intestinal segment, respectively.

Imaging was performed using an A1R HD25 confocal system (Nikon, Tokyo, Japan) combined with a Ti2-Eclipse inverted microscope. Images were acquired using a Nikon Plan Apo λ 20x/0.75 ∞/0.17 WD 1.0 (MRD00205). Plexuses were located using the eyepiece and image acquisition was then performed using the NIS-Element AR 5 software (Nikon). Image acquisition parameters were kept identical for every experiment. They were configured to image large plexus areas in three dimensions (3D) with analyses-compatible spatial resolution, recording speed and dynamic range while minimizing photobleaching. A major challenge to image the ENS in undissected preparations is the inevitable movement of the neurons in response to the contraction of the adjacent smooth muscle (even in the presence of inhibitors to limit movement). While limited drift in the X or Y direction can be corrected in post-processing, movement in the Z direction leads to the creation of artefacts and signal loss that cannot be recovered. To overcome this problem, we performed live 3D image acquisition of the plexuses in order to perform 3D tracking and sampling of fluorescent signals in individual neurons even when they experience a reasonable amount of movement. 3D imaging also allowed us to image and compare Ca^{2+} activity in the myenteric and submucosal plexuses of the small intestine simultaneously. GCaMP6 was excited at 488 nm and its fluorescent emission was collected at 525/550 nm using the Nikon A1-DU4–2 4 Detector Unit (Multi-Alkali PMTs | 12-bit). The field of view size was 648×648 μm and image acquisition was made at 4 frames per second (256×256 pixels, bi-directional). Depending on the region investigated and on the state of the tissue (distended vs relaxed) a total number of 8 to 20 frames was needed to reconstitute the entire plexuses in 3D (Z-step of 4.35 μm). The time resolution ranged from 2 to 5 seconds per consecutive 3D reconstruction. In most experiments, drift of the preparation had to be compensated by visual tracking and manual realignment in real time in the X, Y and Z axes. Despite taking all the above precautions, excessive amounts of drift or sudden movement from the gut segments made image analyses impossible in 10–15 % of the experiments.

Video analyses

Analyses were performed in 3D using Imaris software (RRID:SCR_007370; versions 9.1 to 9.5, Bitplane, Belfast, UK). A breakdown of the video acquisition and analysis workflow is shown on Figs. 1B–D. The 3D video footage was first stabilized semi-automatically and then automatically. We manually tracked a neuron in the centre of the region of interest and realigned the entire footage using this first track as a reference (linear translation) in order to eliminate large movements and drift (generated by live manual realigning). A second stabilization was then performed on that same neuron using the finer built-in “spot” and “tracking” function of the software and realigning the entire footage to that second track.

Neuronal detection and fluorescence quantification were made semi-automatically using the “spot” function of Imaris that models and detects point-like structures and represents them as spheres (Fig. 1B). The software first performed a background subtraction that smooths the 3D image with a Gaussian filter (sigma = Object Diameter / 2) and subtracts this filtered image from the original. The neurons were then automatically detected by setting an

Author Manuscript Author Manuscript Author Manuscript Author Manuscript

estimated X-Y diameter of 12 μm (spots with diameter smaller than this were not detected) and thresholding. The software then created 12 μm spheres overlaid with the centroid of all visible neurons in the 3D images that later served as 3D region of interest for fluorescence intensity measurements.

Spheres representing the same neurons observed at consecutive time points were then assembled as "tracks" using the built-in "autoregressive motion" algorithm that models the motion of each sphere as an autoregressive process. We set up a maximum distance of 10 μm and a maximum gap size of five frames. The maximum distance prevents connections between a sphere and a candidate match if the distance between the predicted future position of the sphere and the candidate position exceeds the maximum distance. In cases where the sphere segmentation failed for some time points, which would break the track, the maximum gap size defines the maximum consecutive time points for which the gap closing algorithm should try to continue the movement of a disappearing object and connects the tracks if it reappeared. We then performed a first automatic sorting of the tracks by discarding all the tracks with a total duration of less than 1 min (artefacts) and all the tracks around the edge of the field of view. Finally, we performed a visual quality control of the tracks and manually excluded all the tracks corresponding to non-neuronal structures.

In Wnt1-GCaMP6 mice, an average of 15 to 35 tracks were randomly selected per experiment (~22 for distal colon myenteric plexus; ~26 for proximal colon myenteric plexus; ~16 for jejunum myenteric plexus and ~13 for jejunum submucosal plexus). In Calb1-GCaMP6 mice, every recordable track present in the field of view (~5 per experiments) was used. Note that it was not possible to accurately discriminate myenteric versus submucosal neurons in Calb1-GCaMP6 mice using our system, hence our data are comprised of responses from neurons in both plexuses. The position (X and Y) and mean intensity over time for each sphere/track was then exported to a spreadsheet. Each individual track was then plotted, and we calculated different calcium dynamic parameters for each individual track (Fig. 1D). The initial fluorescence (F_0) corresponded to the mean fluorescence intensity just before reaction to a stimulus. The maximal fluorescence intensity (F_{max}) corresponded to the highest fluorescence intensity experienced by a neuron after a stimulus. The difference in fluorescence (ΔF) is equal to F_{max}-F_0. Individual neurons were considered responsive to a stimulus when their $\Delta F/F_0$ was greater than 15 %. A $\Delta F/F_0 < 15$ % was considered noise. The "latency" corresponded to the amount of time between introduction of the stimulus and the beginning of the calcium response (determined visually). The "time to peak" (TTP) corresponded to the amount of time needed for a given neuron to go from F_0 to F_{max} and the "decay time" is the amount of time needed for a given neuron to go back to F_0 after reaching F_{max}.

Intraluminal distension

During distension experiments, the intraluminal flow was constant from the oral to the anal end of the segment and was maintained at 10 $mL.h^{-1}$. Non-oxygenated Krebs solution was used as a perfusate to keep the lumen anoxic. In order to generate a physiological level of intraluminal distension, we transiently interrupted the withdrawal from the anal output, while keeping the oral input flowing, resulting in a slow increase of the intraluminal

Author Manuscript Author Manuscript Author Manuscript Author Manuscript

volume. When distension of the jejunum or colon was attained, never exceeding the visual equivalent of the distension generated by the presence of chyme or that of a fecal pellet, the withdrawal on the anal end was resumed. Relaxation was attained by interrupting the perfusion flow while keeping the withdrawal on. The amount of distension was estimated after the experiment by measuring the relative displacement of the neurons inside the field of view. The distance between 36 combinations of neurons was measured over time and averaged for each experiment in the X (longitudinal) and Y (circumferential) axis. Intraluminal distension resulted in an increase in the relative distance between neurons in the Y axis while almost no difference was observed in the X axis. The amount of distension is expressed as the percentage of difference in the distance between neurons over time compared to their initial distance (in the X or Y axis).

Luminal perfusion of nutrients

During nutrient perfusion experiments in isolated jejunal segments, the intraluminal flow (10 $mL.h^{-1}$) and temperature (35–37°C) were maintained constant using PHD 2000 syringe pumps (Harvard Apparatus) combined with 1LG Syringe heaters (New Era Pump Systems Inc., Farmingdale, NY, USA). We used a 3-way valve to interchange Krebs with the nutrient solution, perfused at the same rate in order to keep the mechanical and sheer stress constant during the entire duration of the experiment. Both Krebs and nutrient solution were non-oxygenated. The Nutrient solution was made of 50 % Ensure® (Regular, Abbot, Chicago, IL, USA) v/v mixed in water. The final nutrient solution contained 2 g per 100 mL protein (in the form of milk protein concentrate and soy protein isolate), 1.4 g per 100 mL lipids (in the form of canola, soy and corn oil), 7.4 g per 100 mL sugar (in the form of sucrose and corn maltodextrin) and had the same pH (7.4) and osmolarity (280–290 $mOsm.L^{-1}$) as the Krebs solution. Nutrient perfusion was interrupted by turning the 3-way valve back to the Krebs flow circuit.

Bathing solutions

Krebs buffer (Krebs) contained (in $mmol.L^{-1}$): 121 NaCl, 5.9 KCl, 2.5 $CaCl_2$, 1.2 $MgCl_2$, 1.2 NaH_2PO_4, 14.4 $NaHCO_3$, 11 glucose (Sigma) with 3 $\mu mol.L^{-1}$ nicardipine (Sigma) and 1 $\mu mol.L^{-1}$ scopolamine (Sigma) to inhibit muscle contractions, as previously described (Gulbransen et al., 2012). pH of the Krebs solution was 7.4 after oxygenation (95 % O_2, 5 % CO_2). We purchased tetrodotoxin (TTX) and paxilline from Alomone Labs, Jerusalem, Israel, Cat # T-550 and P-450; veratridine from Calbiochem, San Diego, CA, USA, Cat # 676950; GsMTx4 from AdooQ Bioscience, Irvine, CA, USA, Cat # A16103; 1,1-Dimethyl-4-phenylpiperazinium (DMPP) and gadolinium from Sigma, Cat # D5891 and G7532. In experiments conducted in the presence of TTX, gadolinium, GsMTx4 or paxilline, tissues were bathed in Krebs solution containing one of the inhibitors at the indicated concentration for 10–15 minutes before starting the experiment and throughout the duration of the experiment. For stimulation with veratridine, KCl or DMPP, 10x concentrated stock solutions were prepared in pre-warmed and oxygenated Krebs solution and added to the bath by replacing 10% of the volume with a pipette at the time indicated (black arrows in figures). The immediate concentration obtained in the bath was 10 μM for veratridine, 75 mM for KCl and 100 μM for DMPP. These concentrations were only

Author Manuscript Author Manuscript Author Manuscript Author Manuscript

attained transiently as the chamber was perfused continuously with Krebs solution (with the equivalent of 2–3 times the volume of the chamber being replaced every minute).

Statistics

Statistical analyses were performed with GraphPad Prism version 8 (RRID:SCR_002798; GraphPad Software, San Diego, CA, USA). Ca^{2+} measurements collected from individual neurons were compiled from at least three biological replicates per experimental group and represented as the distribution of neuronal responses above and below the median. Since responsive neurons had very distinctive responses from nonresponsive neurons and since the proportion of responsive neurons was different among experimental groups, the median gave a better representation of the centre of the distribution. For this reason and because of the absence of specific distribution, non-parametric tests were used throughout. Mann-Whitney tests were used to compare two groups (Figs. 2C; 3C, 3F; 6C; 8A; 10E). Kruskal Wallis tests with Dunn's multiple comparison were used to compare three groups (Figs. 8A; 9B, 9C and 9D; 10B). For experiments where the same neurons were followed over time (repeated measures) (Fig. 7E) it was not always possible to collect data at the three distinct time points (due to movement/drift of the preparation). Because some values were missing, we analysed these data by fitting a mixed model (restricted maximum likelihood) and used Holm-Sidak's test for multiple comparisons. We did not run statistical analyses on Figs. 4B and 5C as these data represent a quantitative assessment of inter-regional variability in Ca^{2+} response where no intestinal region could be considered as a reference group. Statistical significance was defined as $P < 0.05$ for all comparisons.

Results

Presence of intestinal contents locally inhibits neuronal activity in the enteric nervous system

We created an integrated system that allowed us to perform live, 3 dimensional calcium (Ca^{2+}) recordings in the ENS of intact intestinal segments of mice. A perfusion chamber was designed to allow the imaging of intestinal segments on an inverted confocal microscope while being able to control the luminal contents and the level of distension inside the lumen (Fig. 1A). Wnt1-GCaMP6 mice were generated in order to quantify and characterize neuronal Ca^{2+} dynamics in individual enteric neurons using three-dimensional (3D) confocal microscopic imaging (Figs. 1B–D). We first investigated neuronal Ca^{2+} activity in the myenteric plexus of intact segments of distal colon in which the luminal contents (fecal pellets) were present. We observed striking differences in neuronal intracellular Ca^{2+} status between the distended pellet regions and undistended interpellet regions (Figs. 2A–C). We observed that in regions of the colon containing a fecal pellet, baseline Ca^{2+} fluorescence was markedly higher than in the interpellet regions (Fig. 2B). Addition of a depolarizing stimulus to the bath (KCl) triggered an increase in neuronal Ca^{2+} fluorescence in the interpellet regions, but remarkably not in the regions of colon containing a fecal pellet (Figs. 2A, 2C and Supplementary Video 1). Similar results were observed with the addition of veratridine, a neurotoxin known to increase nerve excitability and intracellular Ca^{2+} concentrations by preventing the inactivation of voltage-gated sodium ion channels (Fig. 2A and Supplementary Video 2). These responses were lost in regions of the colon

Author Manuscript Author Manuscript Author Manuscript Author Manuscript

containing a fecal pellet, suggesting that the presence of distension renders the overlying enteric neurons unresponsive to depolarization.

We conducted similar investigations in the proximal colon and jejunum, comparing "undistended" intestinal segments, that were free of luminal content, to segments where there was natural distension due to the presence of luminal contents (chyme) (Fig. 3). As before, Ca^{2+} fluorescence was higher in the ENS of segments containing the natural presence of luminal contents than in the undistended segments (Figs. 3B and 3E) and the Ca^{2+} responses following stimulation with KCl or veratridine were markedly reduced or absent in the segments containing luminal contents compared to segments that did not (Figs. 3A, 3C, 3D, and 3F; Supplementary Videos 3–6 and Table 1). Together, these data show that distension generated in the small and large intestines by the presence of luminal contents locally inhibits the responsiveness of enteric neurons by a process involving an alteration of intracellular Ca^{2+} homeostasis.

Regional differences in the organization of neuronal calcium dynamics in the small and large intestine

We next compared KCl-induced Ca^{2+} responses and signal propagation in the ENS between the different intestinal regions (Fig. 4). We decided to focus on KCl response rather than veratridine as it provided more consistency with clearly identifiable neuronal activation patterns. In the distal colon, addition of KCl to the bath led to a rapid increase in Ca^{2+} fluorescence in 94% of the neurons (48/51; n=3; neuronal responsiveness being defined as $\Delta F/F0 > 15$ %). Neuronal responses were characterized by rapid onset and time to peak (TTP, <15s; Figs. 4A and 4B). In the jejunum, an identical stimulus led to a delayed, slow increase in Ca^{2+} fluorescence in 91% of the neurons (58/64; n=3). Neuronal responses were characterized by longer latency to onset, long time to peak (TTP >15s) and longer decay time (Figs. 4A and 4B). In the proximal colon, we observed three patterns of response in responsive neurons (81%, 62/77; n=3): neurons responded either with a rapid increase in Ca^{2+} fluorescence (TTP <15s), a delayed, slow increase (TTP >15s) or a combination of both responses (Figs. 4A and 4B). We did not observe any correlation between the type of response and ganglia location or proximity to caecum. In order to evaluate the organization of the KCl-induced Ca^{2+} propagation within the enteric neuronal networks, we analyzed neurons based on their longitudinal (oral to anal, X) and circumferential (Y) positions and evaluated the temporal organization of their calcium responses (Fig. 4C). We found that there were marked regional differences in the organization of Ca^{2+} propagation between the jejunum and colon. While every neuron was activated almost simultaneously in the distal colon (i.e., in a single frame), Ca^{2+} increases in the jejunum slowly propagate from cell to cell following a circumferential trajectory. The proximal colon presented a mixed response, first displaying a synchronous Ca^{2+} spike followed by a delayed asynchronous Ca^{2+} response across the tissue (Fig. 4C; Supplementary Videos 1, 3 and 5). Overall, these results highlight unique Ca^{2+} dynamics in different neuronal populations along the gut, reflecting distinct regional patterns possibly underlying their specific functional roles.

In order to understand the nature of this Ca^{2+} propagation in the ENS, we conducted a second series of experiments in the presence of the sodium channel blocker tetrodotoxin

Author Manuscript Author Manuscript Author Manuscript Author Manuscript

(TTX). As expected, TTX completely inhibited the response to veratridine in all regions (Fig. 5A). However, we did not observe any differences in KCl-induced Ca^{2+} responses (Fig. 6B and Table 1). Ca^{2+} dynamics and signal propagation maintained their respective tissue specificity in the presence of TTX (Figs. 5B and 5C; Supplementary Videos 7–9), illustrating the ability of enteric neurons to generate Ca^{2+} signals independently of action potential conduction. We conducted an analysis of every neuronal KCl response independently of their treatment groups in order to determine the ability of neurons to respond to a stimulus based on their initial Ca^{2+} level (Fig. 6A). In all three regions of the intestine, we observed that neurons with higher baseline fluorescence tended to have greater increases in fluorescence in response to KCl (Fig. 6B), indicating that the level of the intracellular Ca^{2+} reporter was not a limiting factor in the response to the stimulus (Fig. 6C). In other words, the high-calcium-nonresponsive neurons found in the distended segments are not saturated and are likely made unresponsive through another mechanism.

Intestinal distension finely tunes the organization of neuronal calcium activity

In order to further evaluate the effect of intestinal distension on neuronal activity, we used a perfusion system to generate various levels of intraluminal distension in emptied segments of the distal colon (using non-oxygenated Krebs solution as a perfusate). Distension levels were quantified by measuring the increase in interneuronal distances (displacement) over time across the field of view (Fig. 7A). By generating different levels of colonic distension (from 0 to 75% displacement), we found that the intracellular level of Ca^{2+} in neurons gradually increased with the amount of distension (Fig. 7B). Moreover, when the level of distension resulted in approximately 75% increase in neuronal displacement, enteric neurons were flattened, their baseline Ca^{2+} fluorescence increased and their reactivity to KCl was abolished (Figs. 7A, 7C and Supplementary Video 10). Importantly, when the distal colon was subjected to an intermediate level of distension (~50% displacement), many of the neurons were still responsive to KCl, but their Ca^{2+} dynamics were radically different (Figs. 7D, 7E, 7F and Supplementary Video 11). Recording the same neurons over time, we found that intermediate levels of distension were able to change KCl-induced Ca^{2+} responses in individual neurons from a sharp, rapid Ca^{2+} increase (TTP <15s) to a delayed, slow Ca^{2+} increase (TTP >15s) (Fig. 7E). This phenomenon was fully reversible, as shown by baseline and KCl-induced Ca^{2+} dynamics returning to their initial state when the tissue was allowed to relax (Fig. 7E).

We confirmed these findings by measuring KCl-induced Ca^{2+} responses in segments of distal colon over a single fecal pellet (preserved during colonic resection). Here as well, distension by the fecal pellet inhibited KCl-induced responses, whereas intermediate distension (as observed at the edge of a pellet) changed the neuronal response from a fast Ca^{2+} increase (TTP <15s) in every neuron in the ganglia into a slow Ca^{2+} wave (Fig. 8A and Supplementary Video 12). With intermediate levels of distension (~50% displacement), neurons in the distal colon were activated by KCl in a slow synchronized wave travelling circumferentially (Figs. 8B, 8C and Supplementary Video 13). Analyses of individual neuronal positions at their time of reaction (i.e., when $\Delta F/F0 > 15$ %) showed that neurons were activated across the ENS at a circumferential speed of ~480 $\mu m.min^{-1}$ (Fig. 8D). This circumferential spread was consistently observed and propagation in an

Author Manuscript Author Manuscript Author Manuscript Author Manuscript

oral to anal direction (longitudinal) under these conditions was never observed, suggesting the existence of a circumferential enteric circuit for the propagation of this wave, possibly involving the intrinsic primary afferent neurons (Furness et al., 1998). This circumferential organization was similarly pronounced when examining the position of the neurons at the moment they reached maximal fluorescence intensity (F_{max}) but considerably less pronounced when looking at the time at which their fluorescence returned to baseline (F_0) (Fig. 8D), suggesting that the Ca^{2+} wave originated from the propagation of an unknown activation signal rather than a propagation of Ca^{2+} within the enteric network (through gap junctions for example). Together these data demonstrate that in the ENS of the distal colon, intraluminal distension finely regulates intracellular Ca^{2+} dynamics, ultimately modifying, organizing, or inhibiting neuronal response to a depolarizing stimulus.

Distension is integrated by mechanosensitive channels

We then investigated mechanisms by which the ENS may integrate the mechanical changes induced by distension. The visible deformation of the cell body of the neurons during distension as well as the ubiquitous nature of Ca^{2+} changes prompted us to evaluate which mechanosensitive channels were involved. We measured the distension-induced Ca^{2+} changes in neurons from the distal colon in presence or absence of gadolinium ($GdCl_3$; 50 μM), a non-specific mechano-gated channel blocker(Mueller-Tribbensee et al., 2015) (Fig. 9A). We found that the previously observed increase in intracellular Ca^{2+} induced by distension was suppressed in presence of gadolinium, indicating that mechanosensitive channels are essential for integrating the mechanical changes induced by distension. We repeated this experiment in the presence of more specific inhibitors: the piezo-1 channel blocker GsMTx4 (1 μM) and the $K_{Ca1.1}$ channel blocker paxilline (10 μM) (Sanchez & McManus, 1996; Zhang et al., 2012; Zhu et al., 2022) (Fig. 9A). We did not observe any changes in presence of GsMTx4, however, the distension-induced neuronal Ca^{2+} increase was suppressed in presence of paxilline, indicating that $K_{Ca1.1}$ channels were essential for the integration of mechanical changes. We confirmed these findings by evaluating neuronal Ca^{2+} levels in segments of colon containing fecal pellets and showed that in presence of paxilline ($K_{Ca1.1}$ channel inhibition), the level of Ca^{2+} was no longer elevated in the distended pellet region (Fig. 9B). Moreover, the ability of neurons to react to KCl in the distended area was strikingly recovered in 72% of the neurons in paxilline-treated preparations (Fig. 9B and Table 2). We also performed an independent set of experiment in absence of nicardipine, the L-type voltage-dependent Ca^{2+} channel inhibitor used throughout the study to maintain mechanical stability in our preparations. Here, we were unable to evaluate KCl response due to the instability of the preparations, but we showed a similar increase in neuronal Ca^{2+} in segments of colon containing fecal pellets (mean ± SD neuronal fluorescence 619.4 ± 465.0; 48 neurons, n=3 mice) compared to their respective interpellet regions (mean ± SD neuronal fluorescence 121.5 ± 99.7; 129 neurons, n=3 mice) in absence of nicardipine (panel 1, Fig. 9B). Next, to identify which specific neurons recovered their KCl response in presence of paxilline, we performed similar experiments using ChAT-GCaMP6 mice (Fig. 9C, 9D and Table 2). In these mice, as expected, intracellular Ca^{2+} levels were higher in the pellet region than in the interpellet region and response to KCl was lost in the pellet region. In the presence of paxilline, intracellular Ca^{2+} levels did not increase in the pellet area and the response to KCl was

Author Manuscript Author Manuscript Author Manuscript Author Manuscript

recovered in 89% of the neurons, suggesting that most of the neurons in which the response to KCl is recovered in presence of paxilline were cholinergic neurons. We then evaluated neuronal response to the nicotinic cholinergic agonist DMPP (Fig. 9D and Table 2). Similar to the response to KCl, the response to DMPP was also lost in the distended pellet region; however, it was not recovered in presence of paxilline, despite the low baseline Ca^{2+} level, suggesting that other mechanisms may be at play to inhibit this type of neuronal response. Altogether, these results highlight the critical role played by mechanosensitive channels and more specifically $K_{Ca1.1}$ channels in regulating neuronal ability to respond to depolarizing stimuli according to the amount of colonic distension.

Distension inhibits responses to luminal nutrients

After observing that distension was able to inhibit the neuronal response to different pharmacological stimuli (e.g., KCl, DMPP and veratridine), we then wondered whether similar inhibition would occur with luminal nutrients as a stimulus. We thus perfused segments of jejunum from Wnt1-GCaMP6 with luminal nutrients and measured Ca^{2+} fluorescence in the submucosal and myenteric plexus in the presence or absence of distension. Here we show that intraluminal nutrients triggered an increase in Ca^{2+} in 28% of myenteric (32/113; n=8) and 35% of submucosal neurons (31/89; n=8) (Fig. 10A). This response was substantially reduced when the intestine was concomitantly distended (Figs. 10A, 10B; Supplementary Video 14 and Table 3), suggesting that integration of distension by the ENS renders enteric neurons unresponsive to indirect, chemical stimulation from the intestinal lumen. An interesting feature of the chemosensing of luminal contents is that it was partially TTX-resistant. Indeed, when these experiments were repeated in presence of TTX, we saw a similar increase in Ca^{2+} in 19% of myenteric (12/62; n=4) and 24% of submucosal neurons (10/41; n=4) (Fig. 10B; Supplementary Video 15 and Table 3). We observed a reduction in $\Delta F/F_0$ in the presence of TTX in responsive neurons, but we did not measure any differences in the overall Ca^{2+} dynamics (Figs. 10C and 10D). These data indicate that a subpopulation of neurons is able to detect changes in the chemical composition of the gut lumen independently of fast nerve conduction.

We conducted similar experiments in mice expressing the calcium reporter GCaMP6 only in calbindin-expressing intrinsic primary afferent neurons (Calb1-GCaMP6s)(Qu et al., 2008). Here we observed that 61% of these neurons (in both plexuses) reacted to luminal nutrient stimulation (20/33; n=5) with a Ca^{2+} dynamic similar to that observed in Wnt1-GCaMP6 mice (Figs. 10E and 10F and Supplementary Video 16). Only 19% of these neurons responded when the intestine was distended (3/16; n=3). Taken together, these data indicate that in the absence of distension a subpopulation of enteric neurons, including Calb1 neurons, detects changes in the composition of the luminal contents that results in a dynamic regulation of intracellular Ca^{2+}. In the presence of intestinal distension, intracellular Ca^{2+} levels increase, and luminal stimuli are no longer able to elicit further changes in intracellular Ca^{2+}.

Author Manuscript Author Manuscript Author Manuscript Author Manuscript

Discussion

In the present study we designed an integrated imaging and analysis system that enabled us to evaluate enteric neural network activity in intact intestinal segments from mice. Using this unique tool, we revealed that intestinal distension locally determines the activity and responsiveness of the ENS. Specifically, we showed that intestinal distension inhibited the response to depolarizing stimuli in the ENS. This distension-induced quiescence was observed in all three regions of the gastrointestinal tract that we studied. In the distal colon, we showed that intermediate distension led to a highly dynamic and reversible synchronization of signal propagation within the enteric nervous system. We also found that this distension-induced regulation of intracellular Ca^{2+} and associated neuronal silencing were dependent on mechanosensitive channels and more specifically $K_{Ca1.1}$ channel activity. Finally, we uncovered a distention-sensitive, tetrodotoxin (TTX)-resistant response of enteric neurons to luminal nutrients in the jejunum. These findings reveal novel aspects of enteric neurophysiology not previously observed with traditional approaches to study the ENS.

We have demonstrated that intraluminal distension finely regulates intracellular Ca^{2+} levels in enteric neurons throughout the gut, in a manner independent of action potential generation. In classical models of distension-evoked reflexes, a subpopulation of specialized mechanosensitive neurons detects mechanical distension and then synapses, either directly or via an interneuron, onto excitatory or inhibitory effector neurons (Fung & Vanden Berghe, 2020). However, more recent studies have challenged this idea and suggest that the detection of mechanical changes might be more complex and not limited to mechanosensitive intrinsic neurons, but rather to a much broader population of enteric neurons that change their firing behaviour in response to mechanical stress (Mazzuoli & Schemann, 2012; Mazzuoli-Weber & Schemann, 2015a, 2015b). Here, we discovered that intestinal distension in the small and large intestines affects most of the neurons in the ENS by locally modulating their levels of intracellular Ca^{2+}. Similar observations were made in primary cultures of neurons from the esophagus (Dong et al., 2015) suggesting that this characteristic is conserved along the entire length of the GI tract and thus could represent a ubiquitous feature of enteric neural control. Indeed, intracellular Ca^{2+} is essential for the regulation of neurotransmitter release, membrane excitability and signal propagation in neurons (Brini et al., 2014).

Distension-induced regulation of intracellular Ca^{2+} in enteric neurons could thus represent an additional pathway for the integration of mechanical information by the ENS. The deformation of the ganglion and cell body of the neurons in the distended region was clearly noticeable in our segments and occurred concomitantly with increased intracellular Ca^{2+} levels. This suggests that the observed increase in intracellular Ca^{2+} could be triggered in response to the physical deformation of the neurons. However, what triggers the increase of intracellular Ca^{2+} in response to distension remain to be fully understood. One candidate ion channel is Piezo 1, which is widely expressed in enteric neurons (Mazzuoli-Weber et al., 2019; Drokhlyansky et al., 2020). Previous work from Mazzuoli-Weber et al., found that Piezo 1 was not involved in mechanosensory responses of enteric neurons of the guinea pig ileum (Mazzuoli-Weber et al., 2019). Consistent with this study, we were unable to block the distention-induced elevation of intracellular Ca^{2+} by blocking Piezo 1 channels in

Author Manuscript Author Manuscript Author Manuscript Author Manuscript

the distal colon. Another candidate described by Kunze et al. is the mechanosensitive BK channel ($K_{Ca1.1}$), expressed in intrinsic primary afferent neurons that were inhibited upon compression of their soma (Kunze et al., 2000). However, recent single cell RNA studies of the ENS show that neurons in the myenteric and submucosal plexuses express a wide variety of other mechanosensitive ion channels and receptors that could be candidates for regulating intracellular Ca^{2+} in enteric neurons (Zeisel et al., 2018; Drokhlyansky et al., 2020; Morarach et al., 2021).

Here, using non-specific and specific inhibitors we revealed that mechanosensitive channels are needed for neurons to integrate changes in luminal distention. More specifically, we showed that $K_{Ca1.1}$ channels, but not Piezo1, were essential for the distension-induced increase of intracellular Ca^{2+} in neurons. We also showed that the response was not binary and that intracellular Ca^{2+} levels were finely regulated in relation to the amount of local distension, with functional consequences on neuronal responsiveness. Quite strikingly, inhibition of $K_{Ca1.1}$ channels allowed cholinergic neurons to stay responsive to KCl in presence of high distension, highlighting the essential role of these channels in controlling neuronal excitability. Although it would have been reasonable to think that elevated intracellular Ca^{2+} level could by itself explain the inability of neurons to respond to further stimulus, we demonstrated that it was not the case. We first measured that unresponsive neurons were not saturated and then showed that even when intracellular Ca^{2+} levels were maintained at a low level by blocking $K_{Ca1.1}$ channels, distension still suppressed the neuronal response to the nicotinic cholinergic receptor agonist, DMPP. Thus, diverse and non-redundant mechanisms are in place to control neuronal excitability in the presence of distension. It is worth mentioning that our work did not allow us to evaluate the cellular location of these channels. Since the changes in intracellular Ca^{2+} were concomitant with the distension, we can't exclude that they were secondary to the integration of distension by other cell types such as epithelial cells in the mucosa and smooth muscle cells that also express $K_{Ca1.1}$ channels (Sörensen & Leipziger, 2009; Wang et al., 2010). Lastly, because we performed all our experiments in the presence of the L-type Ca^{2+} channel blocker nicardipine to maintain the mechanical stability of our preparations and because this channel is mechanosensitive (Lyford et al., 2002) and expressed in colonic myenteric neurons (Zeisel et al., 2018; Mazzuoli-Weber et al., 2019), we performed an additional set of experiment in its absence. We were able to validate that the distension-induced increase in intracellular Ca^{2+} was unchanged in presence or absence of nicardipine. It was impossible for us to evaluate KCl response in absence of paxilline due to the instability of the preparation so we cannot completely exclude the possibility that L-type Ca^{2+} channel participate in some of the observed responses thought previous studies have shown that they do not play a role in neurotransmission in the ENS (Wessler et al., 1990; Bian et al., 2004).

Our main finding was that levels of distension that occur physiologically during the passage of a fecal pellet in mice, create sub-regions where the neurons do not respond to depolarization and other sub-regions where the neuronal responses become synchronized. This local regulation could have an important role in the spatiotemporal organization of enteric reflexes, as it would allow selective silencing or synchronization of enteric microcircuits according to the amount of local distension. The main limitation of our system was that it did not allow for an evaluation of the functional consequences of these

Author Manuscript Author Manuscript Author Manuscript Author Manuscript

findings and notably how these distention-induced changes in neuronal activity translate to the regulation of intestinal motility. A recent paper by Spencer et al. revealed that synchronization of large enteric neural assemblies was a determining feature of colonic propulsion (Spencer et al., 2021). Other studies showed that migrating motor complexes were disrupted in colons from mice lacking the β1-subunit of the $K_{Ca1.1}$ channel (Bhattarai et al., 2016) and that stretch-activation of $K_{Ca1.1}$ channels in smooth muscle cells were involved in the stretch-induced relaxation of the colon in rats (Ren et al., 2016).

Here our work suggests that local distention orchestrates neuronal activity by finely regulating the neurons' ability to transport ions. The absence of KCl-induced Ca^{2+} influx in neurons in the fully distended region indicates an inhibition of membrane receptors and/or voltage-dependent ion channels that would otherwise allow Ca^{2+} influx into the neurons. More importantly, the delayed and synchronized response observed with a partial level of distension, as observed at the extremity of a pellet, suggests that depolarization sensitive Ca^{2+} channels are still inhibited in these regions while the activity of other Ca^{2+} transport mechanisms is restored (Smith et al., 2003). A careful examination of the transporter involved in this distention-sensitive alteration of intracellular Ca^{2+} in the ENS is needed and will be the subject of future investigation.

We also showed that integration of signals coming from the lumen by modulation of intracellular Ca^{2+} level was not limited to mechanical stimuli, as we discovered a TTX-resistant Ca^{2+} modulation in a subpopulation of neurons following the perfusion of luminal nutrients. Detection of luminal nutrients has been demonstrated before in the nodose ganglion (Williams et al., 2016; Kaelberer et al., 2018; Pradhananga et al., 2020) and the ENS (Kunze et al., 1995; Bertrand et al., 1997; Sayegh et al., 2004; Fung et al., 2021), but to our knowledge, this is the first demonstration of a TTX-resistant response to luminal nutrients in the ENS. Here we showed that about a third of the neurons in the myenteric and submucosal plexuses responded to luminal nutrients and that more than half of them could do so even in presence of TTX. Interestingly, the nutrient-induced response was blunted in presence of distension, confirming the role of distension in modulating neuronal excitability. Together our work demonstrates the ability of the ENS to monitor and integrate luminal information through changes in intracellular Ca^{2+} that are seemingly independent of action potential generation. We hypothesize that these variations in calcium are essential for the integration of luminal stimuli by locally altering neuronal excitability according to the amount of distension. This regulation could represent a missing link for the integration of noncontinuous mechanical information, such as observed at the level of the colon, where it would allow selective silencing or synchronization of neuronal assemblies needed for the propulsion of pellets with varying size and shape. It could also have a protective role by locally inhibiting or modulating enteric reflexes when the intestine contracts against a luminal blockage. As such, our findings offer a new insight into our understanding of the etiology of intestinal disorders associated with altered luminal distension such as bowel obstruction or chronic constipation.

Finally, our study invites the development of more integrated research approaches to study how the ENS responds to the complex mechanical and chemical inputs it receives from the intestinal lumen. The recent development of optogenetic and chemogenetic tools (Boesmans

Author Manuscript Author Manuscript Author Manuscript Author Manuscript

et al., 2018), as well as the advent of single-cell transcriptomics of enteric neurons (Zeisel et al., 2018; Drokhlyansky et al., 2020; Morarach et al., 2021; Obata et al., 2022), now allows for more integrated and targeted investigations of the ENS (Sharkey & Mawe, 2022). The challenge now is to understand the functional consequences of the present findings on the coordination of the motor, secretory and defensive functions of the gastrointestinal tract.

Supplementary Material

Refer to Web version on PubMed Central for supplementary material.

Acknowledgements

This work was supported by the Live Cell Imaging Laboratory of the Snyder Institute for Chronic Diseases. We thank Drs. Pina Colarusso, Lucy Swift, Katarzyna Wojcik, Andrew Chojnacki, and Rima-Marie Wazen for assistance with image acquisition and analyses and Catherine Keenan for assistance with the breeding and maintenance of the mouse lines. We are extremely grateful to Drs. Jaideep Bains (University of Calgary), Gary Mawe and Grant Hennig (University of Vermont) for their insightful remarks and critical comments on this study.

Funding

This work was supported by grants from the Canadian Institutes of Health Research (PJT 153290, WKM, FDN 148380, KAS), the Natural Sciences and Engineering Research Council of Canada (RGPIN/04321-2018, WKM), the Human Frontier Science Program LT000052/2017-L and Alberta Innovates (J-BC). Additional support was received by NIDDK Diabetic Complications Consortium (RRID:SCR_001415) grants (DK076169 and DK115255, OBB).

Biography

Jean-Baptiste Cavin completed his PhD in gastroenterology and physiology at Paris Diderot University, France during which he studied gastrointestinal and metabolic adaptation after bariatric surgery. He undertook postdoctoral training in the labs of Drs. Sharkey and MacNaughton at the University of Calgary, Canada where he designed novel imaging tools to characterize how enteric neurons respond to intestinal distension and luminal nutrients. Dr. Cavin currently works in the Department of Gastrointestinal Health at the Nestlé Institute of Health Science in Lausanne, Switzerland.

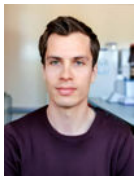

Preedajit Wongkrasant is a postdoctoral fellow working with Drs. MacNaughton and Sharkey. She completed her PhD in physiology at Mahidol University, Thailand, examining the regulation of intestinal epithelial tight junctions. During part of her training, she was a

Author Manuscript Author Manuscript Author Manuscript Author Manuscript

visiting student in the lab of Dr. Kim Barrett, University of California San Diego, USA. Her current focus is on the enteric neural control of digestive functions in health and disease.

Data availability

The authors declare that all the data supporting the findings of this study are available within the paper and its supporting information. Extra data are available from the corresponding authors upon request.

References

Bellono NW, Bayrer JR, Leitch DB, Castro J, Zhang C, O'Donnell T, Brierley SM, Ingraham HA & Julius D (2017). Enterochromaffin cells are gut chemosensors that couple to sensory neural pathways. Cell 170, 185–198.e16. [PubMed: 28648659]

Bertrand PP, Kunze WA, Bornstein JC, Furness JB & Smith ML (1997). Analysis of the responses of myenteric neurons in the small intestine to chemical stimulation of the mucosa. Am J Physiol 273, G422–435. [PubMed: 9277422]

Bhattarai Y, Fried D, Gulbransen B, Kadrofske M, Fernandes R, Xu H & Galligan J (2016). High-fat diet-induced obesity alters nitric oxide-mediated neuromuscular transmission and smooth muscle excitability in the mouse distal colon. Am J Physiol-Gastrointest Liver Physiol 311, G210–G220. [PubMed: 27288421]

Bian X, Zhou X & Galligan JJ (2004). R-type calcium channels in myenteric neurons of guinea pig small intestine. Am J Physiol Gastrointest Liver Physiol 287, G134–142. [PubMed: 14988068]

Boesmans W, Hao MM & Berghe PV (2015). Optical tools to investigate cellular activity in the intestinal wall. J Neurogastroenterol Motil 21, 337–351. [PubMed: 26130630]

Boesmans W, Hao MM & Vanden Berghe P (2018). Optogenetic and chemogenetic techniques for neurogastroenterology. Nat Rev Gastroenterol Hepatol 15, 21–38. [PubMed: 29184183]

Brini M, Calì T, Ottolini D & Carafoli E (2014). Neuronal calcium signaling: function and dysfunction. Cell Mol Life Sci 71, 2787–2814. [PubMed: 24442513]

Dong H, Jiang Y, Dong J & Mittal RK (2015). Inhibitory motor neurons of the esophageal myenteric plexus are mechanosensitive. Am J Physiol Cell Physiol 308, C405–413. [PubMed: 25540174]

Drokhlyansky E, Smillie CS, Van Wittenberghe N, Ericsson M, Griffin GK, Eraslan G, Dionne D, Cuoco MS, Goder-Reiser MN, Sharova T, Kuksenko O, Aguirre AJ, Boland GM, Graham D, Rozenblatt-Rosen O, Xavier RJ & Regev A (2020). The human and mouse enteric nervous system at single-cell resolution. Cell 182, 1606–1622.e23. [PubMed: 32888429]

Fung C, Hao MM, Obata Y, Tack J, Pachnis V, Boesmans W & Berghe PV (2021). Luminal nutrients activate distinct patterns in submucosal and myenteric neurons in the mouse small intestine. bioRxiv DOI: 10.1101/2021.01.19.427232.

Fung C & Vanden Berghe P (2020). Functional circuits and signal processing in the enteric nervous system. Cell Mol Life Sci 77, 4505–4522. [PubMed: 32424438]

Furness JB (2012). The enteric nervous system and neurogastroenterology. Nat Rev Gastroenterol Hepatol 9, 286–294. [PubMed: 22392290]

Furness JB, Kunze WA, Bertrand PP, Clerc N & Bornstein JC (1998). Intrinsic primary afferent neurons of the intestine. Prog Neurobiol 54, 1–18. [PubMed: 9460790]

Grundy D (2015). Principles and standards for reporting animal experiments in The Journal of Physiology and Experimental Physiology. J Physiol 593, 2547–2549. [PubMed: 26095019]

Gulbransen BD, Bashashati M, Hirota SA, Gui X, Roberts JA, MacDonald JA, Muruve DA, McKay DM, Beck PL, Mawe GM, Thompson RJ & Sharkey KA (2012). Activation of neuronal P2X7 receptor-Pannexin-1 mediates death of enteric neurons during colitis. Nat Med 18, 600–604. [PubMed: 22426419]

Han W, Tellez LA, Perkins MH, Perez IO, Qu T, Ferreira J, Ferreira TL, Quinn D, Liu Z-W, Gao X-B, Kaelberer MM, Bohórquez DV, Shammah-Lagnado SJ, de Lartigue G & de Araujo IE (2018). A neural circuit for gut-Induced reward. Cell 175, 887–888. [PubMed: 30340046]

Author Manuscript Author Manuscript Author Manuscript Author Manuscript

Hennig GW, Gould TW, Koh SD, Corrigan RD, Heredia DJ, Shonnard MC & Smith TK (2015). Use of genetically encoded calcium indicators (GECIs) combined with advanced motion tracking techniques to examine the behaviour of neurons and glia in the enteric nervous system of the intact murine colon. Front Cell Neurosci 9, 436. [PubMed: 26617487]

Kaelberer MM, Buchanan KL, Klein ME, Barth BB, Montoya MM, Shen X & Bohórquez DV (2018). A gut-brain neural circuit for nutrient sensory transduction. Science 361, eaat5236.

Kunze WA, Mao Y, Wang B, Huizinga JD, Ma X, Forsythe P & Bienenstock J (2009). Lactobacillus reuteri enhances excitability of colonic AH neurons by inhibiting calcium-dependent potassium channel opening. J Cell Mol Med 13, 2261–2270. [PubMed: 19210574]

Kunze WAA, Bornstein JC & Furness JB (1995). Identification of sensory nerve cells in a peripheral organ (the intestine) of a mammal. Neuroscience 66, 1–4. [PubMed: 7637860]

Kunze WAA, Clerc N, Furness JB & Gola M (2000). The soma and neurites of primary afferent neurons in the guinea-pig intestine respond differentially to deformation. J Physiol 526, 375–385. [PubMed: 10896726]

Lai NY, Musser MA, Pinho-Ribeiro FA, Baral P, Jacobson A, Ma P, Potts DE, Chen Z, Paik D, Soualhi S, Yan Y, Misra A, Goldstein K, Lagomarsino VN, Nordstrom A, Sivanathan KN, Wallrap A, Kuchroo VK, Nowarski R,… Chiu IM. (2020). Gut-innervating nociceptor neurons regulate Peyer's patch microfold cells and SFB levels to mediate Salmonella host defense. Cell 180, 33–49.e22. [PubMed: 31813624]

Lyford GL, Strege PR, Shepard A, Ou Y, Ermilov L, Miller SM, Gibbons SJ, Rae JL, Szurszewski JH & Farrugia G (2002). alpha(1C) (Ca(V)1.2) L-type calcium channel mediates mechanosensitive calcium regulation. Am J Physiol Cell Physiol 283, C1001–1008. [PubMed: 12176756]

Mazzuoli G & Schemann M (2012). Mechanosensitive enteric neurons in the myenteric plexus of the mouse intestine. PLoS ONE 7, e39887.

Mazzuoli-Weber G, Kugler EM, Bühler CI, Kreutz F, Demir IE, Ceyhan OG, Zeller F & Schemann M (2019). Piezo proteins: incidence and abundance in the enteric nervous system. Is there a link with mechanosensitivity? Cell Tissue Res 375, 605–618. [PubMed: 30324494]

Mazzuoli-Weber G & Schemann M (2015a). Mechanosensitivity in the enteric nervous system. Front Cell Neurosci 9, 408. [PubMed: 26528136]

Mazzuoli-Weber G & Schemann M (2015b). Mechanosensitive enteric neurons in the guinea pig gastric corpus. Front Cell Neurosci 9, 430. [PubMed: 26578888]

Morarach K, Mikhailova A, Knoflach V, Memic F, Kumar R, Li W, Ernfors P & Marklund U (2021). Diversification of molecularly defined myenteric neuron classes revealed by single-cell RNA sequencing. Nat Neurosci 24, 34–46. [PubMed: 33288908]

Mueller-Tribbensee SM, Karna M, Khalil M, Neurath MF, Reeh PW & Engel MA (2015). Differential contribution of TRPA1, TRPV4 and TRPM8 to colonic nociception in mice. PloS One 10, e0128242.

Obata Y, Castaño Á, Boeing S, Bon-Frauches AC, Fung C, Fallesen T, de Agüero MG, Yilmaz B, Lopes R, Huseynova A, Horswell S, Maradana MR, Boesmans W, Vanden Berghe P, Murray AJ, Stockinger B, Macpherson AJ & Pachnis V (2020). Neuronal programming by microbiota regulates intestinal physiology. Nature 578, 284–289. [PubMed: 32025031]

Obata Y, Castaño Á, Fallesen TL, Bon-Frauches AC, Boeing S, Huseynova A, McCallum S, Lasrado R, Heanue TA & Pachnis V (2022). Molecular profiling of enteric nervous system cell lineages. Nat Protoc 17, 1789–1817. [PubMed: 35676375]

Pradhananga S, Tashtush AA, Allen-Vercoe E, Petrof EO & Lomax AE (2020). Protease-dependent excitation of nodose ganglion neurons by commensal gut bacteria. J Physiol 598, 2137–2151. [PubMed: 32134496]

Qu Z-D, Thacker M, Castelucci P, Bagyánszki M, Epstein ML & Furness JB (2008). Immunohistochemical analysis of neuron types in the mouse small intestine. Cell Tissue Res 334, 147–161. [PubMed: 18855018]

Ren J, Xin F, Liu P, Zhao H-Y, Zhang S-T, Han P, Huang H-X & Wang W (2016). Role of BKCa in stretch-induced relaxation of colonic smooth muscle. BioMed Res Int 2016, 9497041.

Sanchez M & McManus OB (1996). Paxilline inhibition of the alpha-subunit of the high-conductance calcium-activated potassium channel. Neuropharmacol 35, 963–968.

Author Manuscript Author Manuscript Author Manuscript Author Manuscript

Sayegh AI, Covasa M & Ritter RC (2004). Intestinal infusions of oleate and glucose activate distinct enteric neurons in the rat. Auton Neurosci Basic Clin 115, 54–63.

Sharkey KA & Mawe GM (2022). The enteric nervous system. Physiol Rev; DOI: 10.1152/physrev.00018.2022.

Smith TK, Kang SH & Vanden Berghe P (2003). Calcium channels in enteric neurons. Curr Opin Pharmacol 3, 588–593. [PubMed: 14644009]

Sörensen MV & Leipziger J (2009). The essential role of luminal BK channels in distal colonic K+ secretion. J Med Investig JMI 56 Suppl, 301.

Spencer NJ, Hennig GW & Smith TK (2002). A rhythmic motor pattern activated by circumferential stretch in guinea-pig distal colon. J Physiol 545, 629–648. [PubMed: 12456839]

Spencer NJ & Hu H (2020). Enteric nervous system: sensory transduction, neural circuits and gastrointestinal motility. Nat Rev Gastroenterol Hepatol 17, 338–351. [PubMed: 32152479]

Spencer NJ, Travis L, Wiklendt L, Costa M, Hibberd TJ, Brookes SJ, Dinning P, Hu H, Wattchow DA & Sorensen J (2021). Long range synchronization within the enteric nervous system underlies propulsion along the large intestine in mice. Commun Biol 4, 955. [PubMed: 34376798]

Suarez AN, Hsu TM, Liu CM, Noble EE, Cortella AM, Nakamoto EM, Hahn JD, de Lartigue G & Kanoski SE (2018). Gut vagal sensory signaling regulates hippocampus function through multi-order pathways. Nat Commun 9, 2181. [PubMed: 29872139]

Wang W, Huang H, Hou D, Liu P, Wei H, Fu X & Niu W (2010). Mechanosensitivity of STREX-lacking BKCa channels in the colonic smooth muscle of the mouse. Am J Physiol-Gastrointest Liver Physiol 299, G1231–G1240. [PubMed: 20864656]

Wessler I, Dooley DJ, Werhand J & Schlemmer F (1990). Differential effects of calcium channel antagonists (omega-conotoxin GVIA, nifedipine, verapamil) on the electrically-evoked release of [3H]acetylcholine from the myenteric plexus, phrenic nerve and neocortex of rats. Naunyn Schmiedebergs Arch Pharmacol 341, 288–294. [PubMed: 2333100]

Williams EK, Chang RB, Strochlic DE, Umans BD, Lowell BB & Liberles SD (2016). Sensory neurons that detect stretch and nutrients in the digestive system. Cell 166, 209–221. [PubMed: 27238020]

Zeisel A et al. (2018). Molecular architecture of the mouse nervous system. Cell 174, 999–1014.e22. [PubMed: 30096314]

Zhang J, Halm ST & Halm DR (2012). Role of the BK channel (KCa1.1) during activation of electrogenic K+ secretion in guinea pig distal colon. Am J Physiol Gastrointest Liver Physiol 303, G1322–1334. [PubMed: 23064759]

Zhu T, Kala S, Guo J, Wu Y, Chen H, Zhu J, Wong KF, Cheung CP, Huang X, Zhao X, Lei T, Yang M & Sun L (2022). The mechanosensitive ion channel Piezo1 modulates the migration and immune response of microglia. bioRxiv DOI: 10.1101/2022.06.17.496581.

Author Manuscript Author Manuscript Author Manuscript Author Manuscript

Key point summary:

- How the enteric nervous system of the gastrointestinal tract responds to luminal distension remains to be fully elucidated.
- Here we show that intestinal distension modifies intracellular calcium levels in the underlying enteric neuronal network, locally and reversibly silencing neurons in the distended regions.
- In the distal colon, luminal distension is integrated by specific mechanosensitive channels and coordinates the dynamics of neuronal activation within the enteric network.
- In the jejunum, distension suppresses the neuronal calcium response induced by luminal nutrients.
- Physiological levels of distension dynamically regulate the excitability of enteric neuronal circuits.

Author Manuscript Author Manuscript Author Manuscript Author Manuscript

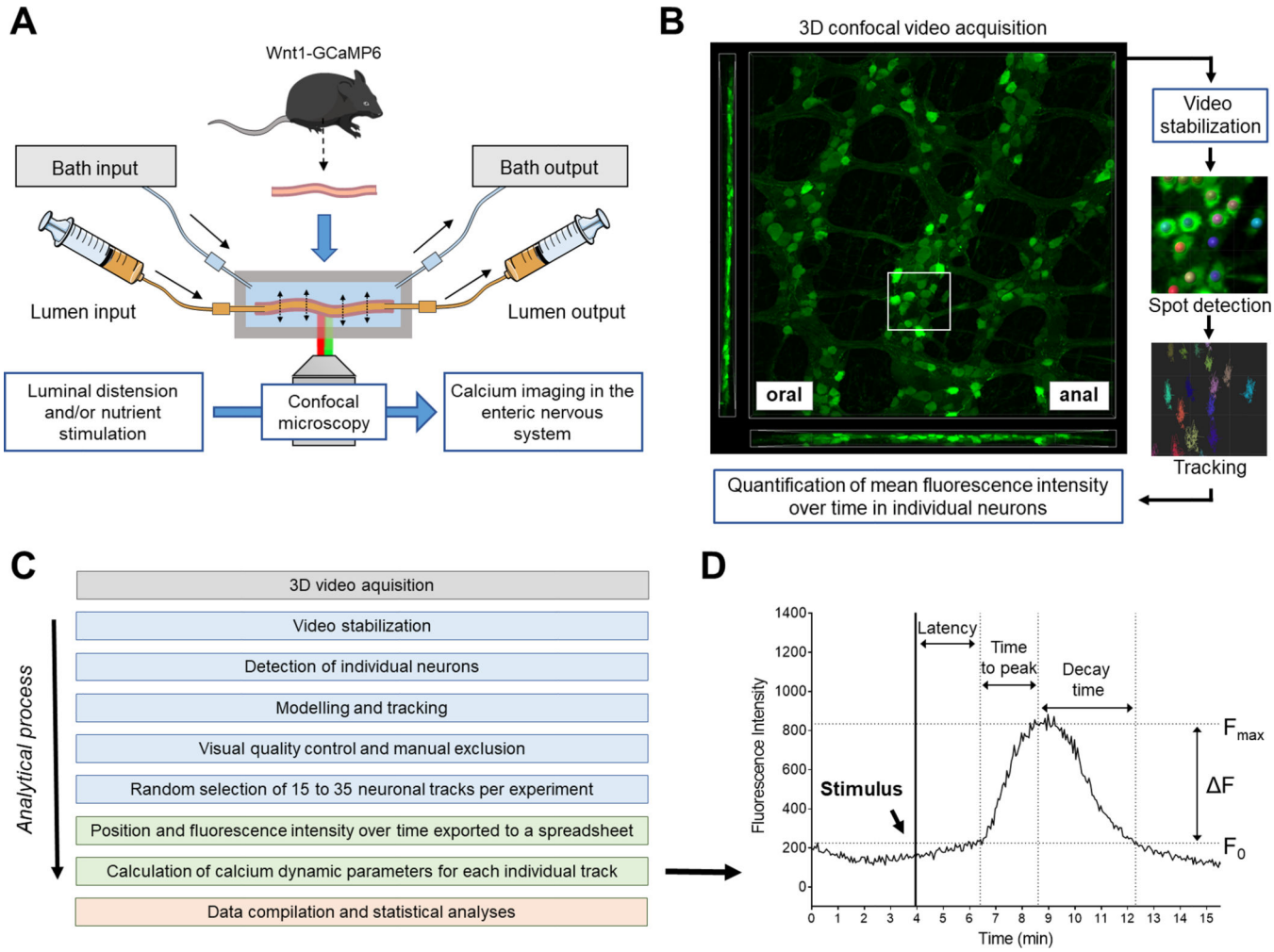

Figure 1.

Schematic illustrations of the perfusion chamber, video acquisition and image analysis workflow. **(A)** Intact intestinal segments from Wnt1-GCaMP6, Calb1-GCaMP6 or Chat-GCaMP6 mice were mounted in a custom-made chamber allowing control of the luminal contents and the level of distension of the preparation. The chamber was placed on the stage of an inverted confocal microscope to perform live cell imaging of enteric neurons without having to dissect the tissue. **(B)** Three-dimensional (3D) video acquisition of the neuronal plexuses was performed and mean fluorescence intensity over time in individual neurons was quantified. **(C)** Image analysis workflow (from top to bottom): Blue boxes correspond to analyses made using 3D imaging software Imaris (Bitplane); Green and red boxes correspond to analyses made with Microsoft Excel and Graphpad Prism, respectively. **(D)** Illustration of the different calcium dynamic parameters measured or calculated for each individual neuron. The initial fluorescence (F_0) corresponds to the mean fluorescent intensity immediately before reaction to a stimulus. The maximal intensity (F_{max}) corresponds to the highest intensity experienced by a neuron after a stimulus. The difference in fluorescence (ΔF) is equal to F_{max}-F_0. Individual neurons were considered responsive to a stimulus when their $\Delta F/ F_0$ was greater than 15 %; $\Delta F/F_0 < 15$ % was

Author Manuscript Author Manuscript Author Manuscript Author Manuscript

considered noise. The “latency” corresponded to the amount of time between introduction of the stimulus and the beginning of the calcium response (determined visually). The “time to peak” corresponded to the amount of time needed for a given neuron to go from F_0 to F_{max} and the “decay time” is the amount of time needed for a given neuron to go back to F_0 after reaching F_{max}.

Author Manuscript Author Manuscript Author Manuscript Author Manuscript

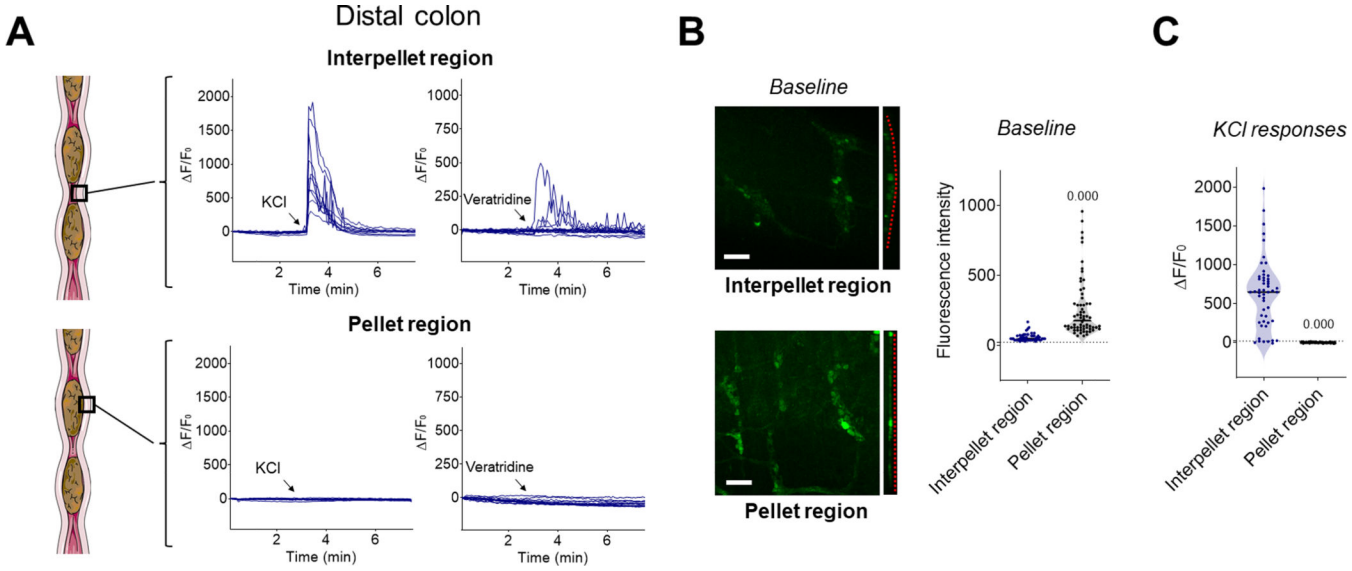

Figure 2.

The presence of fecal pellets locally inhibits neuronal Ca^{2+} responses in the enteric nervous system of the distal colon. **(A)** Representative traces of Ca^{2+} fluorescence changes in individual neurons from the myenteric plexus of intact segments of distal colon containing fecal pellets in response to KCl (75 mM, left panels) or veratridine (10 μM, right panels) added to the bath (arrows) while imaging neurons in the interpellet region (upper panels) or in the region of a fecal pellet (lower panels). Note the absence of responses in the distended pellet region. **(B)** Representative fields of view of the myenteric plexus of the distal colon (left) and quantification of baseline fluorescence intensity in individual neurons (right). Note the flattening of the myenteric plexus (dotted red line) and brighter neurons in the region of the colon distended by a fecal pellet. n = 3 mice per group. Scale bar: 100 μm. **(C)** Quantification of $\Delta F/F_0$ in individual neurons of the distal colon in response to KCl added to the bath. n = 3 mice per group. p-value compared to interpellet region using Mann-Whitney test.

Author Manuscript Author Manuscript Author Manuscript Author Manuscript

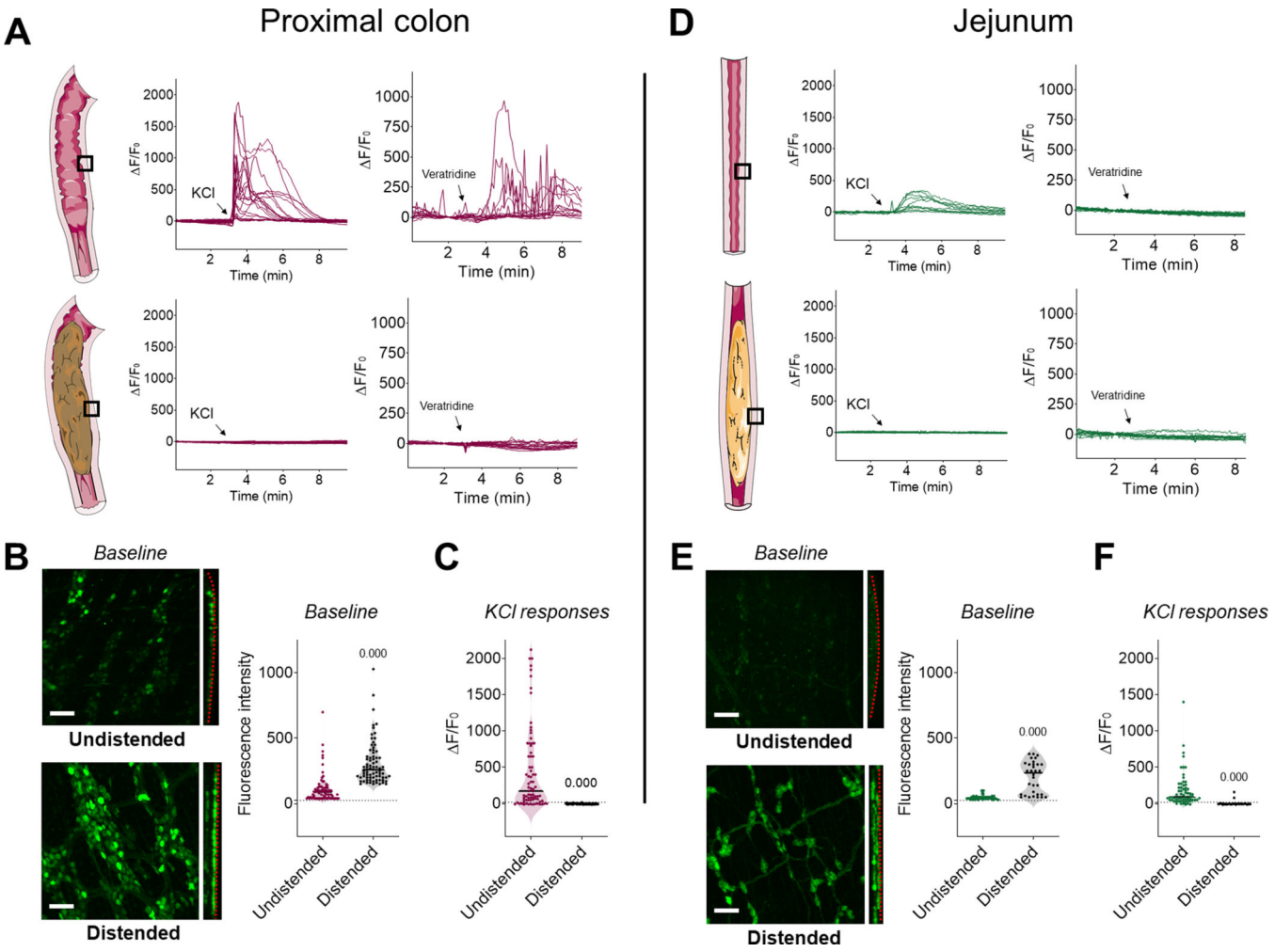

Figure 3.

The presence of luminal contents inhibits enteric neuronal Ca^{2+} responses in the jejunum and proximal colon. **(A)** Representative traces of Ca^{2+} fluorescence changes in individual neurons from the myenteric plexus of intact segments of proximal colon in response to KCl (75 mM, left panels) or veratridine (10 μM, right panels) added to the bath (arrows) while imaging neurons in the undistended state (upper panels) or when the colon was distended with fecal matter (lower panels). Note the absence of responses in the distended region. **(B)** Representative fields of view of the myenteric plexus of the proximal colon (left panels) with quantification of baseline fluorescence intensity in individual neurons (right panels). Note the flattening of the myenteric plexus (dotted red line) and brighter neurons in the distended segment compared to the undistended one. Scale bar: 100 μm. **(C)** Quantification of $\Delta F/F_0$ in individual neurons from the proximal colon in response to KCl added to the bath. n = 3 mice per group. p-value compared to undistended segments using Mann-Whitney test. **(D)** Ca^{2+} fluorescence changes in individual neurons from the myenteric plexus of intact segments of jejunum containing luminal contents in response to KCl (left panels) or veratridine (right panels) added to the bath (arrows) while imaging neurons in the undistended region (upper panels) or where the jejunum was distended by the presence of chyme (lower panels). Note the absence of responses when the jejunum is

Author Manuscript Author Manuscript Author Manuscript Author Manuscript

distended. **(E)** Representative field of view of the enteric nervous system of the jejunum (left) with quantification of baseline fluorescence intensity in individual neurons (right). Note the flattening of the plexuses (dotted red line) and brighter neurons in the distended segment compared to the undistended one. Scale bar: 100 μm. n = 3 mice per group. **(F)** Quantification of $\Delta F/F_0$ in individual neurons from the jejunum in response to KCl added to the bath. n = 3 mice per group. p-value compared to undistended segments using Mann-Whitney test.

Author Manuscript
Author Manuscript
Author Manuscript
Author Manuscript

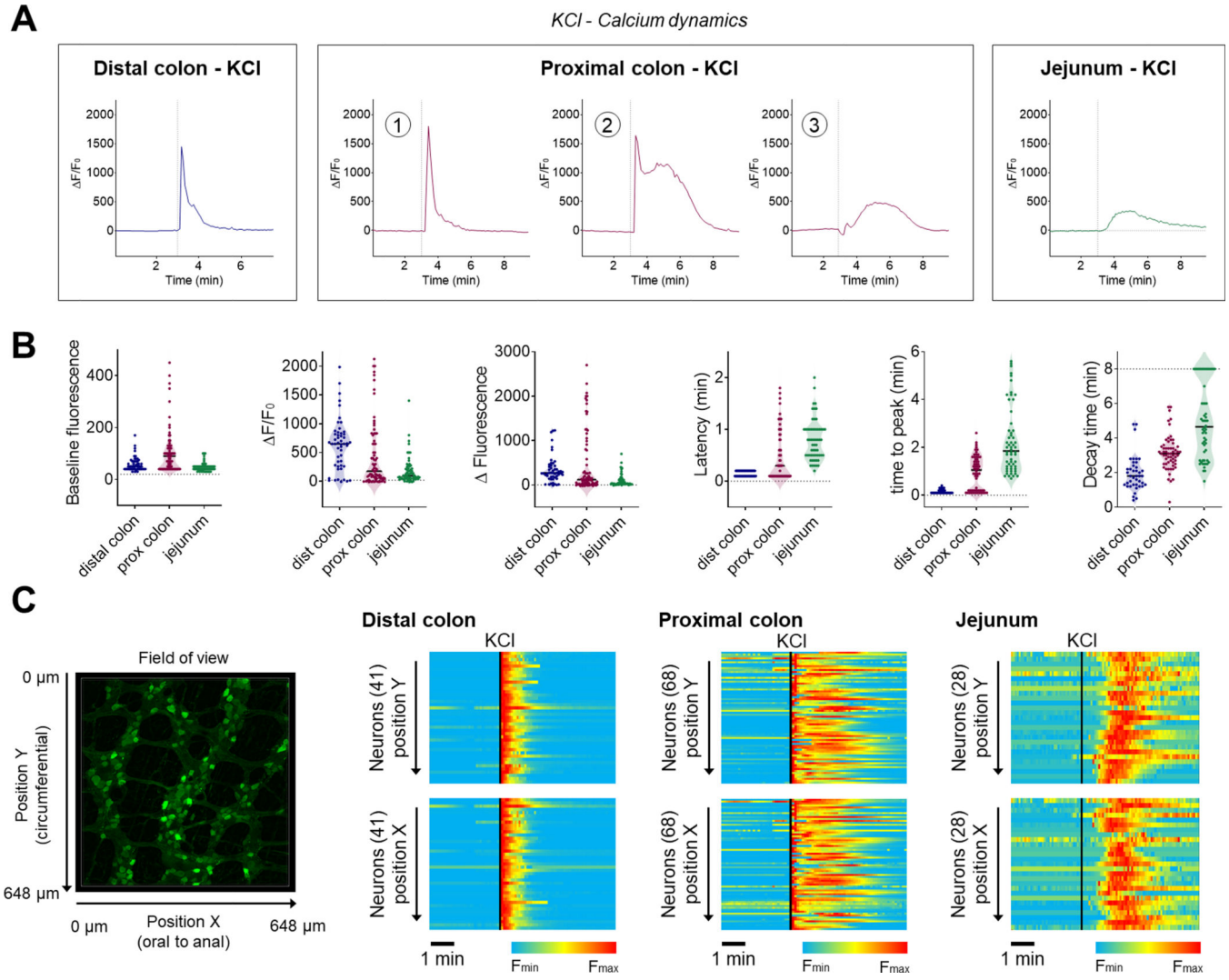

Figure 4.

Ca^{2+} dynamics in the myenteric plexus in response to KCl. **(A)** Representative traces of KCl-induced neuronal Ca^{2+} responses in the different regions of the gut in the absence of luminal contents. In the distal colon, rapid responses (time to peak [TTP] <15s; left box) were always observed, while in the jejunum, slow responses were observed (TTP >15s right box). In contrast, in the proximal colon 3 different types of response were observed: (1) fast response (~26%), (2) combined response (~59%), (3) slow response (~15%) (middle box). **(B)** Quantification of baseline (left panel) and KCl-induced Ca^{2+} responses and dynamics (other panels) in the three regions of the gut in the absence of luminal contents. n=3 mice per group. Note the inter-region variability and specificity in Ca^{2+} dynamics among the various regions of the gut. **(C)** Organization of neuronal responses across the field of view in different regions of the gut in the absence of luminal contents. Individual neuronal responses to KCl (75 mM, black vertical line) were compiled and organized according to their Y (circumferential) or X (oral to anal) position in the field of view (left panel). Each horizontal line represents an individual neuron from the same field of view with color coded activity. Neurons were organized from top to bottom according to their relative Y (upper panels)

Author Manuscript Author Manuscript Author Manuscript Author Manuscript

or X (lower panels) position to highlight any organization in Ca^{2+} propagation within the enteric neuronal networks. Note the simultaneous neuronal activation in response to KCl in the distal colon (left panels) and the delayed circumferential activation in the jejunum (right panels), while neurons in the proximal colon show both fast and/or delayed responses (middle panels).

Author Manuscript
Author Manuscript
Author Manuscript
Author Manuscript

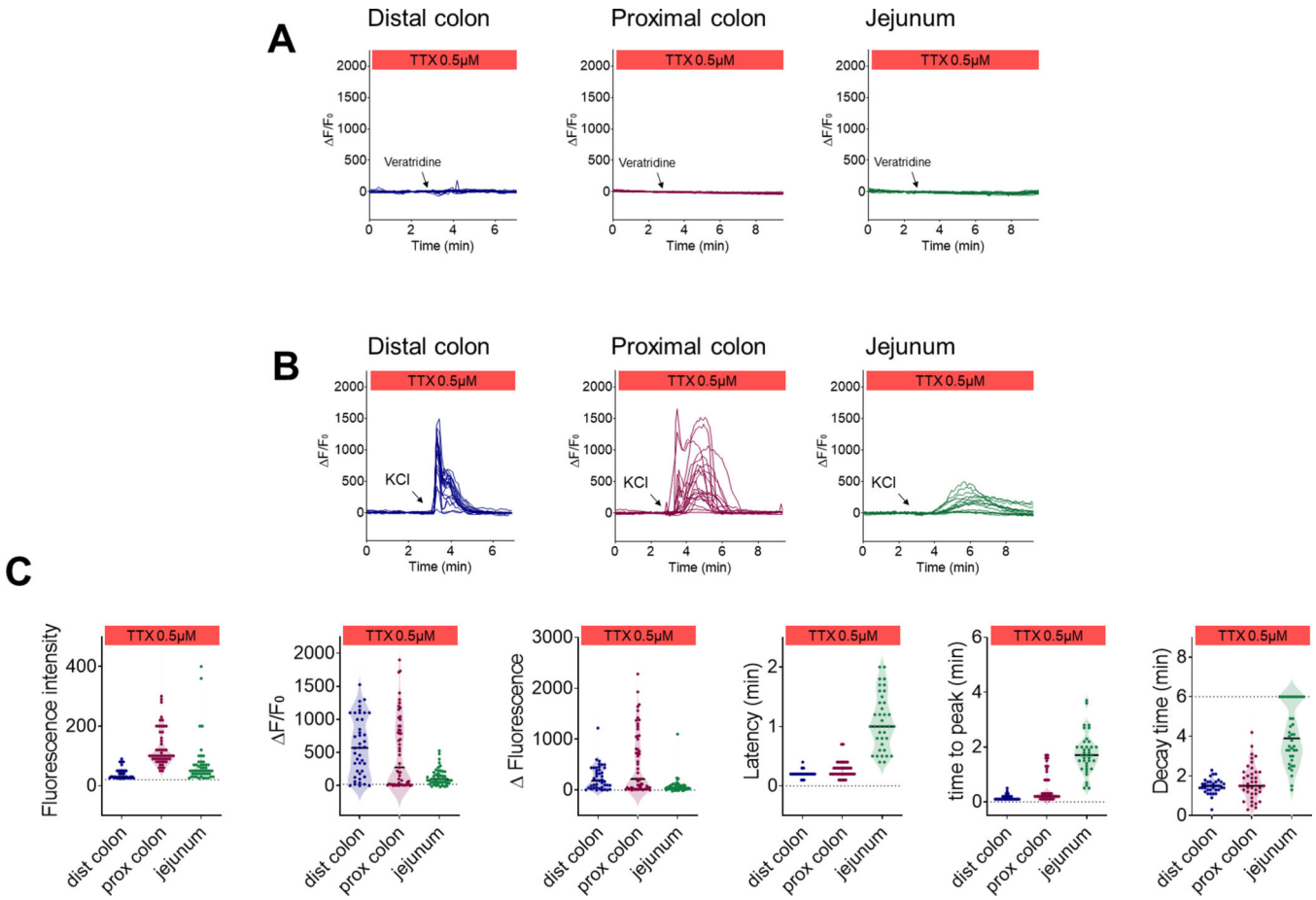

Figure 5.

Ca^{2+} responses in the myenteric plexus in the presence of tetrodotoxin (TTX). **(A)** Neuronal response to veratridine (10 μM) added to the bath (arrow). Note the absence of responses to veratridine in the presence of TTX. **(B)** Neuronal response to KCl (75 mM) added to the bath (arrow). Note that the response is preserved in the presence of TTX. **(C)** Quantification of baseline (left panel) and KCl-induced Ca^{2+} responses and dynamics in the different regions of the gut in the absence of luminal contents and in the presence of TTX (other panels). n=2 per group and per intestinal segment (n=6 mice total); The inter-region variability and specificity of Ca^{2+} dynamics were virtually identical in the presence of TTX (compare to Fig. 4).

Author Manuscript Author Manuscript Author Manuscript Author Manuscript

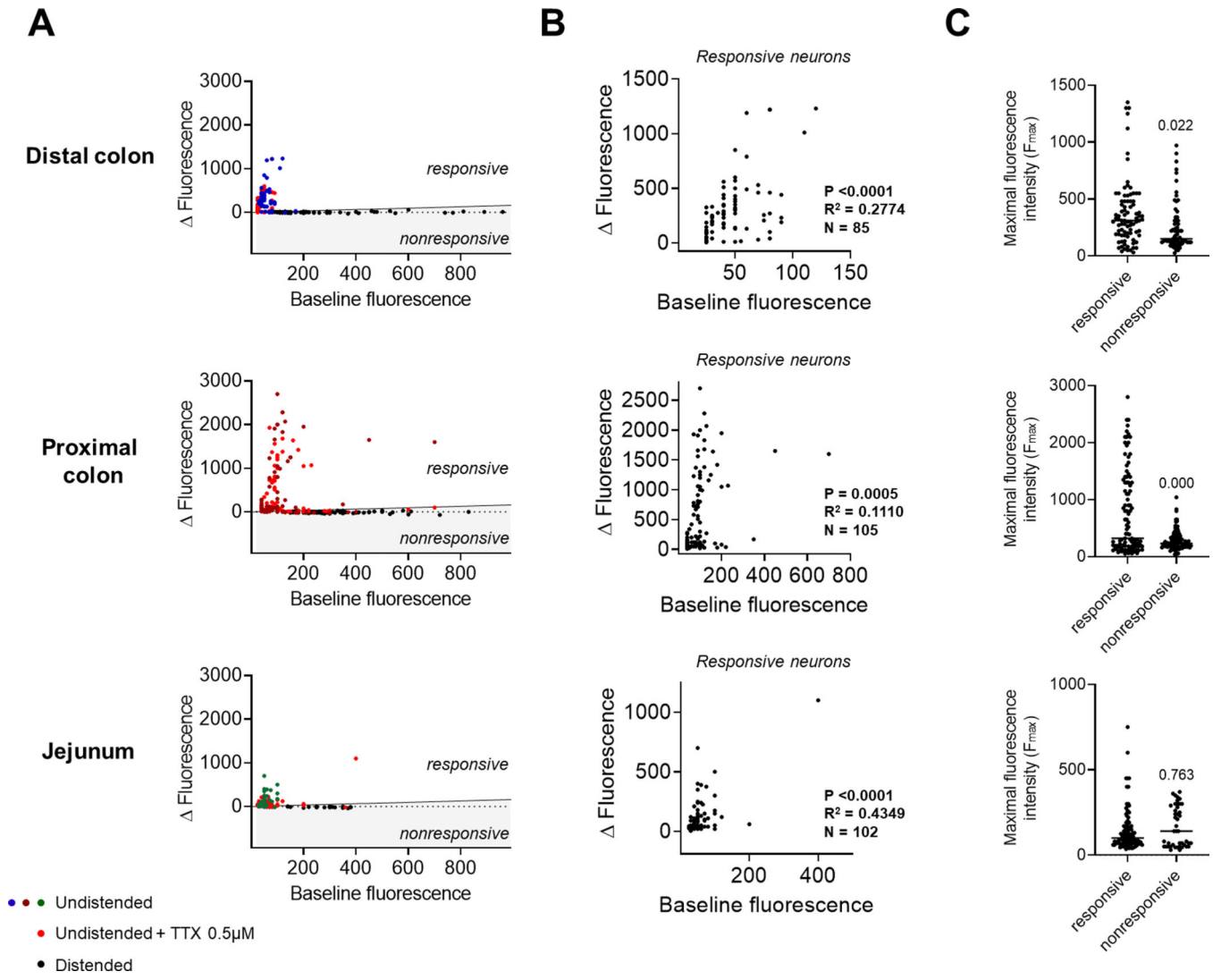

Figure 6.

Ca^{2+} properties in responsive and nonresponsive neurons. **(A)** Individual neuronal responses to KCl (75 mM) obtained from 8 independent experiments in the distal colon (upper panel), proximal colon (middle panel) or jejunum (lower panel) were classified as responsive ($\Delta F/F_0$ > 15 %; black line) or nonresponsive ($\Delta F/F_0$ < 15 %) independently of their treatment groups (colors shown for illustration purposes) and analyzed separately. **(B)** Correlation between baseline fluorescence and ΔF in responsive neurons from the distal colon (upper panel), proximal colon (middle panel) or jejunum (lower panel). Note that neurons with higher baseline fluorescence tend to have a greater ΔF in response to KCl. **(C)** Comparison of maximal fluorescence intensity recorded in individual neurons between responsive and nonresponsive neurons from the distal colon (upper panel), proximal colon (middle panel) or jejunum (lower panel); n=8 mice. p-value compared to responsive neurons using Mann-Whitney test.

Author Manuscript Author Manuscript Author Manuscript Author Manuscript

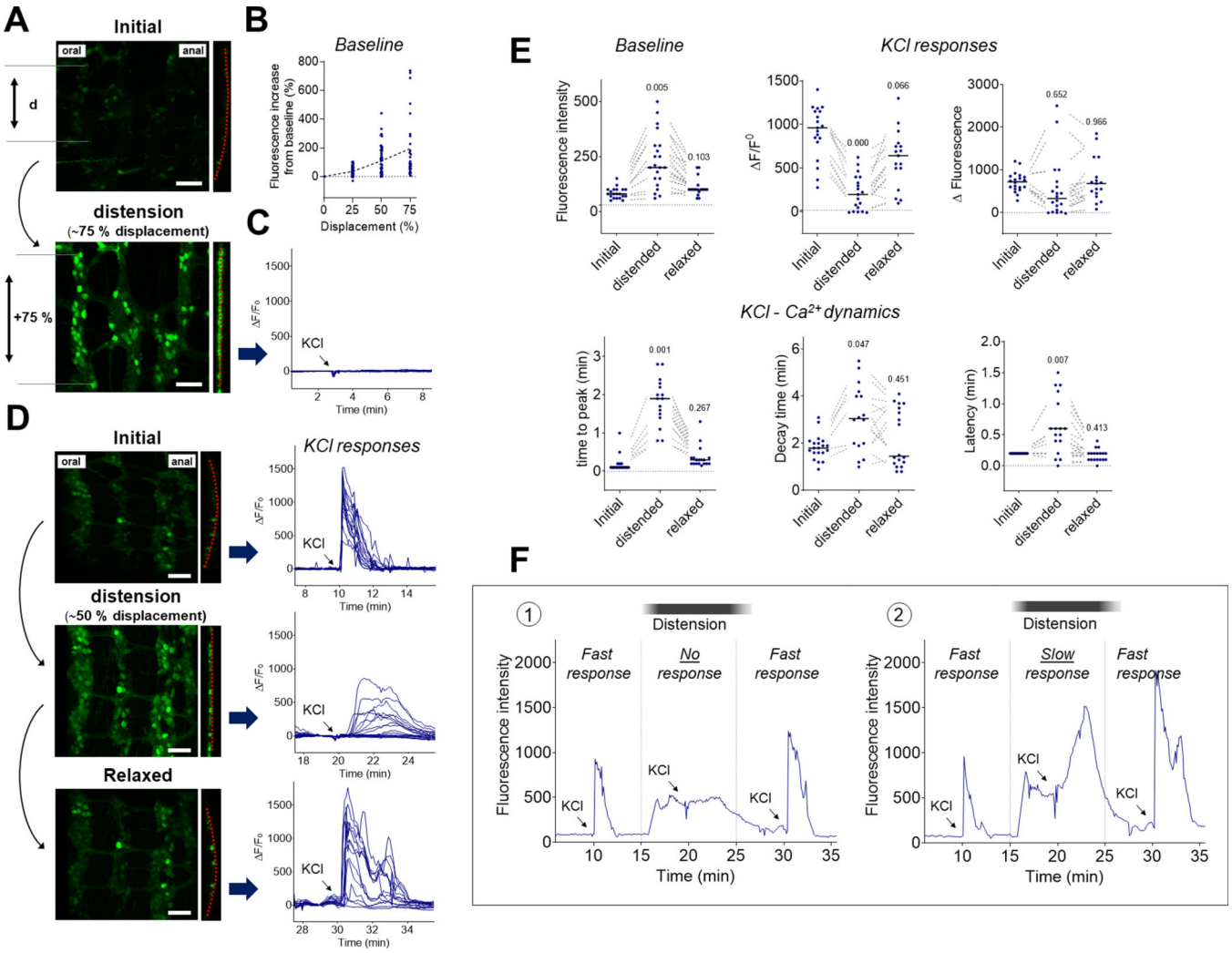

Figure 7.

Distension finely tunes neuronal Ca^{2+} dynamics in the distal colon. Segments of distal colon were distended to different levels and neuronal Ca^{2+} dynamics in individual neurons were assessed over time. **(A)** Representative fields of view of the myenteric plexus before (upper panel) and during (lower panel) intraluminal distension. Note the increased distance between neurons (d) during distension, corresponding to an average of 75 % of their initial distance (displacement) which is associated with the flattening of the myenteric plexus (dotted red line) and brightening of the neurons in response to distension. Scale bar: 100 µm. **(B)** Quantification of changes in fluorescence intensity in individual neurons followed over time during gradual distension of colonic segments (n=4). The dashed line represents the evolution of the mean fluorescence at the different distension steps. **(C)** representative Ca^{2+} fluorescence traces of individual neurons in response to KCl (75 mM) during high distension, corresponding to an average of 75 % of their initial distance (displacement). Note the absence of responses. **(D)** Representative fields of view of the myenteric plexus before distension (upper panel), during intermediate distension (middle panel) and after relaxation (lower panel). Note the increased distance between neurons during intermediate

Author Manuscript Author Manuscript Author Manuscript Author Manuscript

distension, corresponding to an average of ~50 % of their initial distance (displacement). We also observed a flattening of the myenteric plexus (dotted red line) and brightening of the neurons in response to distension, with a return to initial shape and brightness after relaxation. Scale bar: 100 μm. Right panels show representative traces of neuronal Ca^{2+} fluorescence in the same individual neurons in response to KCl added to the bath (arrow) before distension (upper panel), during distension (middle panel) and after relaxation (lower panel). Note the reversible alteration of neuronal Ca^{2+} dynamics when the distal colon is slightly distended. **(E)** Quantification of baseline fluorescence in individual neurons followed over time (upper left panel), $\Delta F/F_0$ (upper centre panel), ΔFluorescence (upper right panel), time to peak (lower left panel), decay time (lower centre panel) and latency (lower right panel) in response to KCl added to the bath. The dotted lines connect the same neurons recorded before, during and after intestinal distension. Note the reversible changes in Ca^{2+} responses and dynamics observed among the same neurons in response to distension. p-value compared to initial values using a mixed-effects model with Holm-Sidak's test for multiple comparisons. **(F)** Representative traces of individual neuronal Ca^{2+} responses in the myenteric plexus of intact segments of distal colon in response to multiple applications of KCl (75 mM, arrows) while the tissue is transiently distended (black bars). Some neurons were inhibited in the presence of distension (1) while some others were still responsive (2). Note the slower increase in fluorescence observed in the presence of distension in responsive neurons (2) and the reversibility of the response when the tissue is allowed to relax (1 and 2).

Author Manuscript Author Manuscript Author Manuscript Author Manuscript

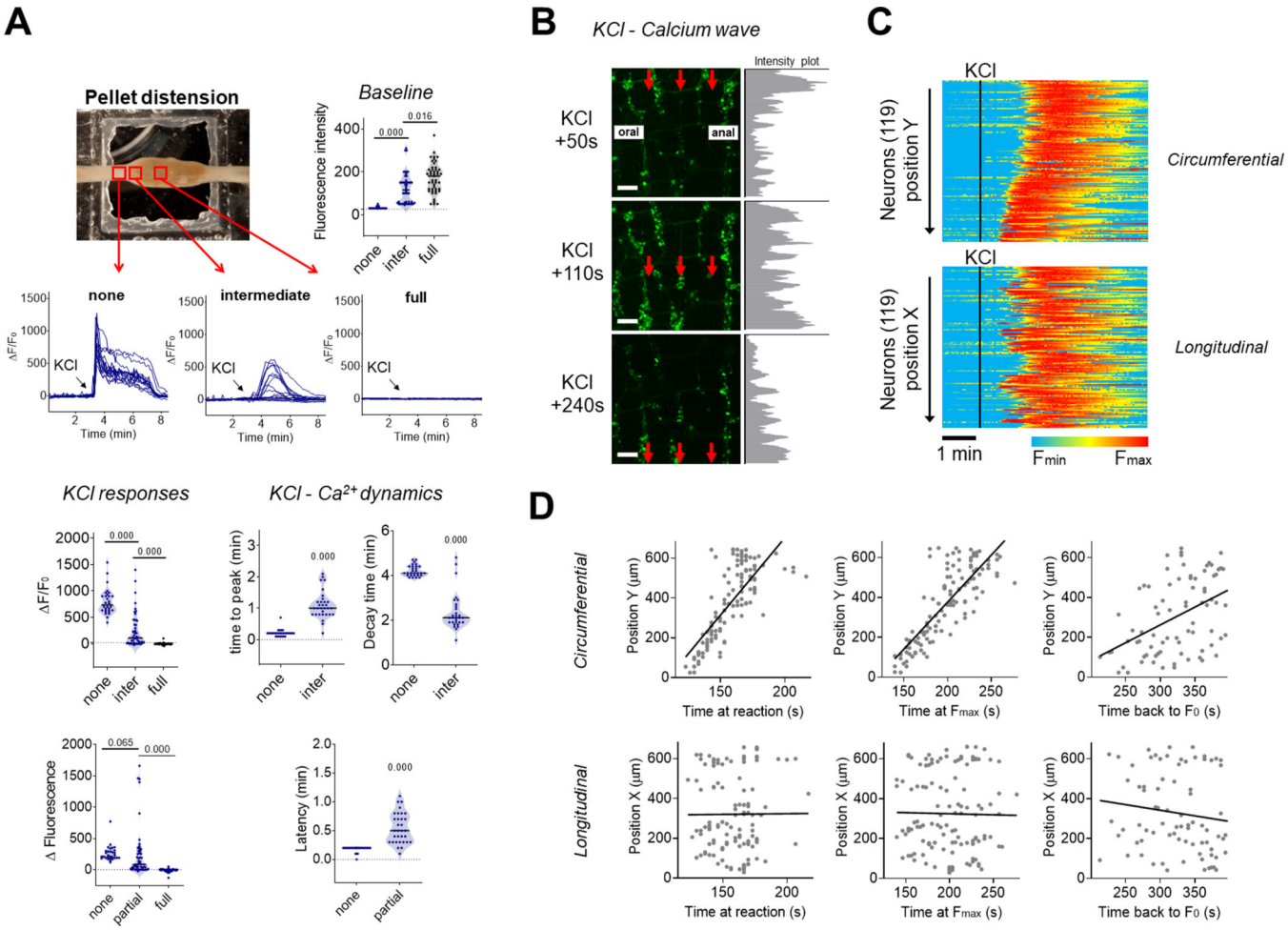

Figure 8.

Ca^{2+} dynamics in the distal colon. **(A)** Neuronal Ca^{2+} fluorescence measured at three distinct sublocations of the distal colon over a fecal pellet. Red boxes represent the different imaging sites where the distension generated by the pellet was none, intermediate or full (upper left panel). Quantification of baseline fluorescence in individual neurons from these different sublocations (upper right panel). Representative traces of individual neuronal Ca^{2+} responses to KCl in the different sublocations (central panels). Quantification of KCl responses ($\Delta F/F_0$ and ΔF; lower left panels) and Ca^{2+} dynamics (time to peak, decay time and latency) in individual neurons (lower right panels). n = 3 mice. p-value using Kruskal Wallis test with Dunn's multiple comparisons (3 groups) or Mann-Whitney test (2 groups). **(B)** Representative images of a circumferential Ca^{2+} wave propagating in a moderately distended segment of distal colon after addition of KCl in the bath. Red arrows highlight the direction of the propagation. Grey intensity plots on the right show the horizontal sum of pixel intensities across the corresponding images. Scale bar: 100 µm. **(C)** Compilation of 119 individual neuronal responses to KCl (black vertical line) in a moderately distended segment of distal colon. Each horizontal line represents an individual neuron with color-coded activity. Neurons were organized according to their relative Y (circumferential; upper panels) or X (oral to anal; lower panels) position to illustrate the

Author Manuscript Author Manuscript Author Manuscript Author Manuscript

circumferential organization of the response. **(D)** Correlation between different events of the neuronal response to KCL and their position along the Y (circumferential, upper panels) or X axis (oral to anal, lower panels) in the field of view. Left panels show the time at which individual neurons started to react, centre panels show the time at which individual neurons reached maximal intensity and right panels show the time a which they went back to their initial fluorescence. Linear regressions (black lines) were used to calculate the average speed at which the Ca^{2+} wave was propagating in the circumferential (~480 $\mu m.min^{-1}$) or oral to anal direction (~6 $\mu m.min^{-1}$). Note the greater amount of circumferential organization (distance of individual dots from black line in the upper panels) when neurons initially react and when they reach maximal intensity but not when they come back to initial fluorescence.

Author Manuscript Author Manuscript Author Manuscript Author Manuscript

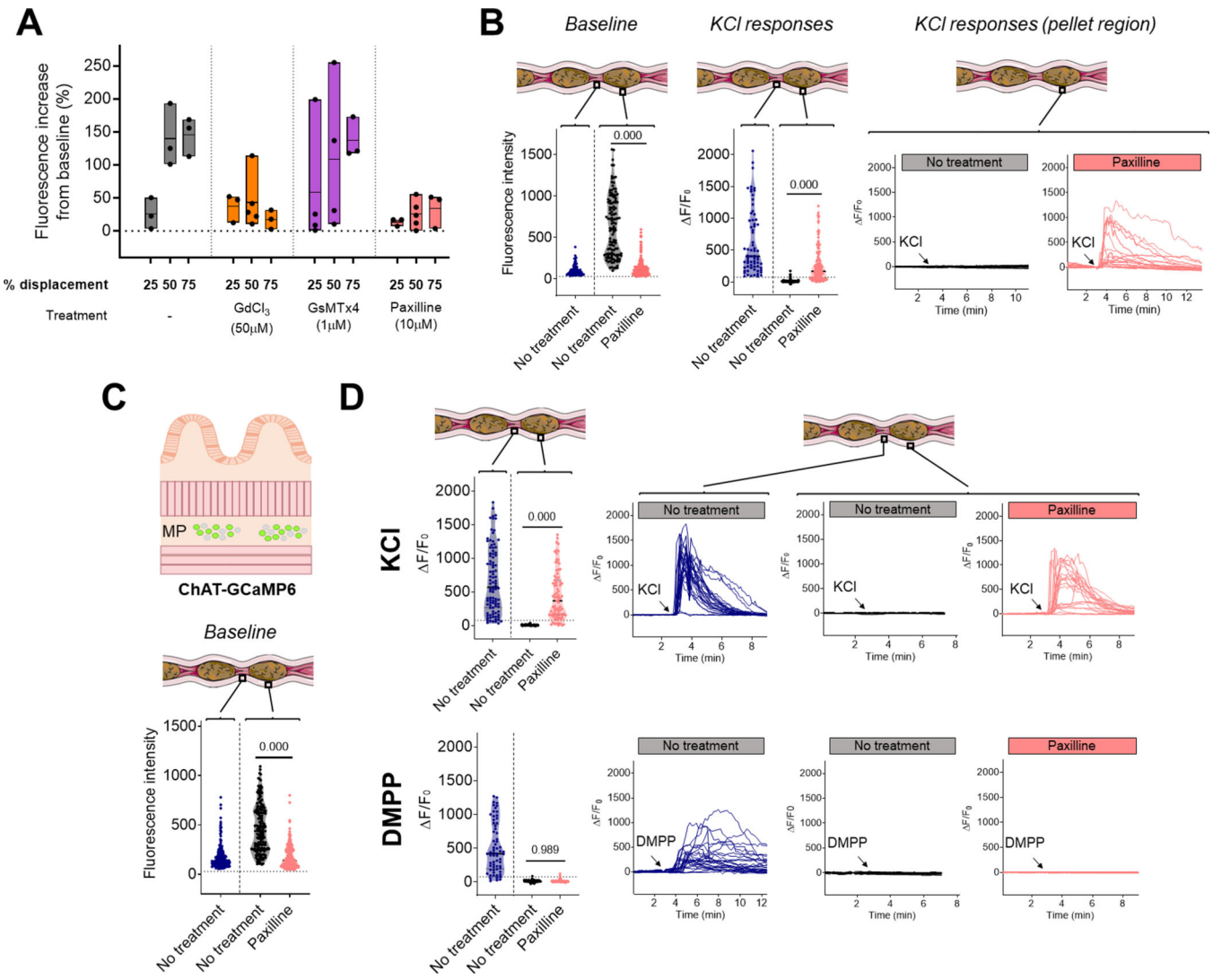

Figure 9.

Distension is integrated by mechanosensitive channels. **(A)** Quantification of the average changes in neuronal fluorescence intensity with different level of colonic distension compared to baseline (dotted line). Measurements were performed in presence of different mechanosensitive channel blockers. Each dot represents the neuronal average for one distal colonic segment. Horizontal bars represent the mean fluorescence for each distension levels. **(B)** Ca^{2+} responses to KCl in the interpellet and pellet region of the distal colon of Wnt1-GCaMP6 mice in presence or absence of $K_{Ca1.1}$ channel blocker paxilline. Quantification of baseline fluorescence intensity in individual neurons (left panel); $\Delta F/F_0$ in response to KCl in individual neurons (middle panel) and representative traces of Ca^{2+} responses to KCl in individual neurons of distended segments of colon (right panel). Note the maintenance of low baseline fluorescence when the colon is distended in presence of paxilline and the associated recovery of KCl response in the distended region. n=3–5 mice per group. p-value using Kruskal Wallis test with Dunn's multiple comparisons. **(C)** Ca^{2+} responses to KCl were recorded in ChAT-GCaMP6 mice to evaluate responses in cholinergic neurons.

Author Manuscript Author Manuscript Author Manuscript Author Manuscript

Baseline fluorescence intensity was quantified in individual neurons in the interpellet and pellet region of the distal Colon in presence or absence of paxilline. n=6–7 mice per group. p-value using Kruskal Wallis test with Dunn's multiple comparisons. Note the maintenance of low baseline fluorescence when the colon is distended in presence of paxilline. **(D)** Responses to KCl (upper panels) and DMPP (lower panels) in the distal colon of ChAT-GCaMP6 mice. Response in the interpellet region was compared to the pellet region in presence or absence of paxilline; with $\Delta F/F_0$ in individual neurons (left panels) and representative traces of Ca^{2+} responses in individual neurons (right panels). Note the recovery of KCl response but not of DMPP response in presence of paxilline in the distended region. n=3–4 mice per group; p-value using Kruskal Wallis test with Dunn's multiple comparisons.

Author Manuscript Author Manuscript Author Manuscript Author Manuscript

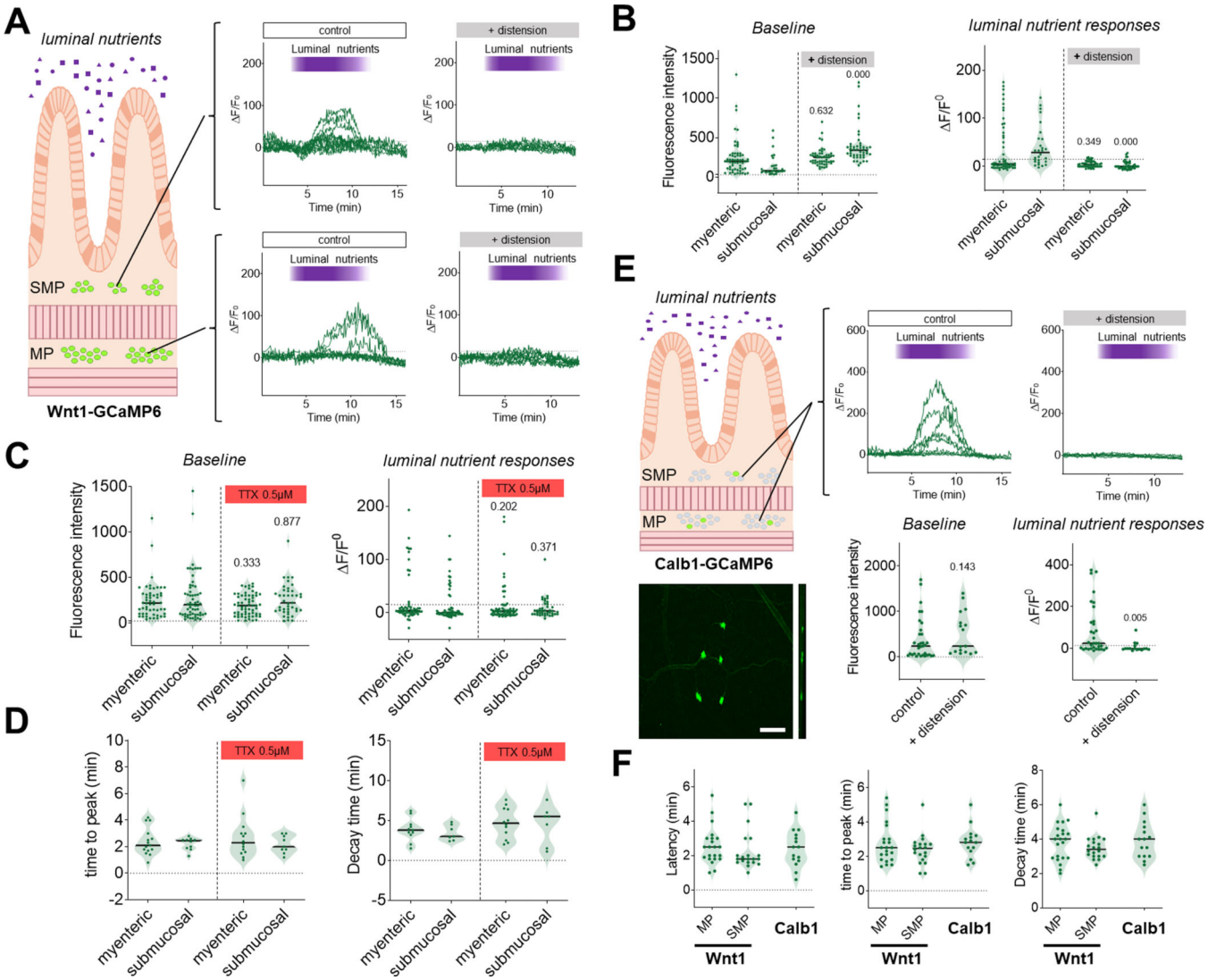

Figure 10.

Distension inhibits neuronal Ca^{2+} responses to luminal nutrients in the jejunum. **(A-B)** Neuronal Ca^{2+} responses to luminal nutrients in the jejunum in presence or absence of intestinal distension. The submucosal and myenteric plexuses were analyzed separately. **(A)** Representative traces of Ca^{2+} responses to luminal nutrients in individual neurons from the submucosal (upper panels) or myenteric (lower panels) plexuses of intact segments of jejunum in the presence (left panels) or absence (right panels) of luminal distension. Note the absence of response to nutrients when the jejunum is distended. **(B)** Quantification of baseline fluorescence intensity (left panel) and $\Delta F/F_0$ (right panel) in response to luminal nutrients in the presence or absence of intestinal distension in individual neurons from the myenteric or submucosal plexus. n=3 mice per group; p- value compared to respective undistended segment using Kruskal Wallis tests with Dunn's multiple comparison. **(C-D)** Neuronal Ca^{2+} responses to luminal nutrients in the jejunum in the presence or absence of TTX (0.5 µM). **(C)** Quantification of baseline fluorescence intensity in individual neurons from the myenteric or submucosal plexus in the presence or absence of TTX (left panel) and

Author Manuscript Author Manuscript Author Manuscript Author Manuscript

$\Delta F/F_0$ in individual neurons from the myenteric or submucosal plexus in response to luminal nutrients in the presence or absence of TTX (right panel); n=4–5 mice per group. **(D)** Quantification of time to peak and decay time in responding neurons after stimulation with luminal nutrients in the presence or absence of TTX. n=4–5 mice per group. Note the similar nutrient induced Ca^{2+} dynamic was observed in responding neurons in the presence or absence of TTX. **(E)** Ca^{2+} responses to luminal nutrients were recorded in Calb1-GCaMP6 mice in order to evaluate responses in intrinsic primary afferent neurons (representative field of view in lower left panel). Note the limited number of neurons in the field of view. Scale bar: 100 μm. Representative traces of Ca^{2+} responses to luminal nutrients in individual Calb1-GCaMP6 neurons of intact segments of jejunum in the presence (upper middle panel) or absence (upper right panel) of luminal distension. Note the absence of response to nutrients when the jejunum is distended. Quantification of baseline fluorescence intensity in individual neurons in presence or absence of intestinal distension (left panel) and $\Delta F/F_0$ in response to luminal nutrients in individual neurons in presence or absence of intestinal distension (right panel). n=3–5 mice per group. p-value compared to control group using Mann-Whitney test. **(F)** Quantification of latency, time to peak and decay time in responding neurons from Wnt1-GCaMP6 (myenteric or submucosal) and Calb1-GCaMP6 (all neurons) after stimulation with luminal nutrients. n=4–5 mice per group. Note the similar nutrient induced Ca^{2+} dynamics observed in responding neurons.

Author Manuscript

Author Manuscript

Author Manuscript

Author Manuscript

Table 1.

Neuronal responses to 75 mM KCl added to the bath in different regions of the gut. Percentage of responsive neurons ($\Delta F/F_0 > 15$ %) in the presence or absence of luminal contents and in the presence of tetrodotoxin (TTX, 0.5 μM).

	Distal colon			**Proximal colon**			**Jejunum**		
	Interpellet	**Pellet**	**0.5 μM TTX (Interpellet)**	**Empty**	**Distended**	**0.5 μM TTX (Empty)**	**Empty**	**Distended**	**0.5 μM TTX (Empty)**
% of responsive neurons (*responsive/recorded*)	**94.1 %** (*48/51*)	**0 %** (*0/65*)	**92.9 %** (*39/42*)	**80.5 %** (*62/77*)	**1.3 %** (*1/77*)	**78.2 %** (*43/55*)	**90.6 %** (*58/64*)	**4.8 %** (*2/42*)	**84 %** (*42/50*)
Standard deviation	5.9	0	13.3	15.3	2.1	18.7	3.8	9.6	8.5
Number of mice per group	3	3	2	3	3	2	3	3	2

Author Manuscript

Author Manuscript

Author Manuscript

Author Manuscript

Table 2.

Myenteric neuronal responses to KCl (75 mM) or DMPP (100 μM) in the distal colon of Wnt1-GCaMP6 or ChAT-GCAMP6 mice. Percentage of responsive neurons ($\Delta F/F_0 > 75$ %) in the presence or absence of fecal pellet and in the presence of paxilline (10 μM).

	Wnt1-GCaMP6			**ChAT-GCaMP6**					
	KCl (75 mM)			**KCl (75 mM)**			**DMPP (100 μM)**		
	Interpellet	**Pellet**	**10 μM paxilline (Pellet)**	**Interpellet**	**Pellet**	**10 μM paxilline (Pellet)**	**Interpellet**	**Pellet**	**10 μM paxilline (Pellet)**
% of responsive neurons *(responsive/ recorded)*	**100 %** (68/68)	**4.3 %** (4/93)	**72.4 %** (92/127)	**94.7 %** (90/95)	**0 %** (0/82)	**89.2 %** (74/83)	**93.8 %** (61/65)	**1.2 %** (1/83)	**2.2 %** (2/93)
Standard deviation	0	7.7	21.5	10.3	0	10.7	9.6	1.8	6.7
Number of mice per group	3	3	4	3	3	3	3	4	4

Author Manuscript

Author Manuscript

Author Manuscript

Author Manuscript

Table 3.

Neuronal responses to luminal nutrients in the myenteric and submucosal plexus of the jejunum. Percentage of responsive neurons ($\Delta F/F_0 > 15$ %) in the presence or absence of luminal distension and in the presence of tetrodotoxin (TTX, 0.5 μM).

	Jejunum					
	Myenteric			**Submucosal**		
	Control	**Distension**	**0.5 μM TTX**	**Control**	**Distension**	**0.5 μM TTX**
% of responsive neurons (*responsive/recorded*)	**28.3 %** (32/*113*)	**6.5 %** (4/*62*)	**19.4 %** (12/*62*)	**34.8 %** (*31/89*)	**7.1 %** (4/*56*)	**24.4 %** (10/*41*)
Standard deviation	23	11	12.8	34.2	10	15.5
Number of mice per group	8	3	4	8	3	4